


Review

Open Access



Imaging evaluation of sinonasal tract neoplasms

Vikramjeet Singh¹ , Alexander Khalaf², Giang-Kim Nguyen³, Richard Fagan⁴, Shirley Y. Su⁵, Kim Learned⁶, Kuang-chun Jim Hsieh⁷

¹Department of Radiology, Baylor College of Medicine, Houston, TX 77030, USA.

²Department of Neuroradiology, Division of Diagnostic Imaging, The University of Texas MD Anderson Cancer Center, Houston, TX 77030, USA.

³Department of Radiology, Baylor College of Medicine, Houston, TX 77030, USA.

⁴Department of Radiology, Baylor College of Medicine, Houston, TX 77030, USA.

⁵Department of Head and Neck Surgery, The University of Texas MD Anderson Cancer Center, Houston, TX 77030, USA.

⁶Department of Neuroradiology, Division of Diagnostic Imaging, The University of Texas MD Anderson Cancer Center, Houston, TX 77030, USA.

⁷Department of Radiology, Baylor College of Medicine, Houston, TX 77030, USA.

Correspondence to: Dr. Vikramjeet Singh, Department of Radiology, Baylor College of Medicine, One Baylor Plaza - BCM360, Houston, TX 77030, USA. E-mail: vikramjeet.singh1029@gmail.com

How to cite this article: Singh V, Khalaf A, Nguyen GK, Fagan R, Su SY, Learned K, Hsieh KJ. Imaging evaluation of sinonasal tract neoplasms. *Mini-invasive Surg.* 2025;9:28. <https://dx.doi.org/10.20517/2574-1225.2024.75>

Received: 24 Sep 2024 **First Decision:** 20 May 2025 **Revised:** 9 Jul 2025 **Accepted:** 21 Aug 2025 **Published:** 29 Aug 2025

Academic Editor: Giulio Belli **Copy Editor:** Pei-Yun Wang **Production Editor:** Pei-Yun Wang

Abstract

The objectives of this article are to review the essential anatomy of the paranasal sinuses, describe computed tomography (CT) and magnetic resonance (MR) imaging approaches to the evaluation of paranasal sinus neoplasms, discuss imaging features of common sinonasal tract tumors, and examine systemic staging and surveillance of sinonasal neoplasms using FDG PET/CT and DOTATATE PET/CT.

Keywords: Imaging, sinonasal, neoplasms, sinonasal tract, CT, MRI, PET

INTRODUCTION

Sinonasal malignancies encompass a diverse group of rare and aggressive tumors with distinct imaging features, histopathological characteristics, and clinical behaviors. Early and accurate diagnosis, precise staging, and close monitoring are critical for developing effective treatment strategies and improving patient outcomes. This review highlights the role of imaging-based tumor mapping and tissue characterization in diagnosing sinonasal malignancies. It also discusses imaging modalities such as FDG PET/computed



© The Author(s) 2025. **Open Access** This article is licensed under a Creative Commons Attribution 4.0 International License (<https://creativecommons.org/licenses/by/4.0/>), which permits unrestricted use, sharing, adaptation, distribution and reproduction in any medium or format, for any purpose, even commercially, as long as you give appropriate credit to the original author(s) and the source, provide a link to the Creative Commons license, and indicate if changes were made.



tomography (CT) and DOTATATE PET/CT, highlighting their importance in improving diagnostic accuracy, evaluating treatment response, and detecting recurrence.

Key anatomy of the paranasal sinuses

The anterior skull base consists of the ethmoid, frontal, and sphenoid bones. It plays an essential role in maintaining communication between the paranasal sinuses and the nasal cavity. Malignancy in this region can disrupt normal respiratory and mucociliary clearance pathways. A detailed understanding of the ostiomeatal unit (OMU) drainage system is crucial for surgeons managing sinonasal diseases and tumors. The most common histologic type of sinonasal cancer is squamous cell carcinoma (SCC)^[1].

The ethmoid bone contains three key components. The cribriform plate forms the roof of the nasal cavity. The ethmoidal labyrinth contains the ethmoid air cells and extends to the lamina papyracea, which forms the lateral nasal wall. The perpendicular plate contributes to the nasal septum [Figure 1]^[2].

The paranasal sinuses share drainage pathways that ultimately terminate in the nasal cavity. The anterior and posterior ethmoid air cells are separated by the basal lamella of the middle turbinate. The anterior ethmoid air cells drain into the middle meatus before reaching the nasal cavity, while the posterior ethmoid air cells drain into the superior meatus and then the sphenoethmoidal recess (SER). The frontal sinus drains through the frontal recess into the ethmoid infundibulum and then into the middle meatus^[2].

The anterior ethmoid, maxillary, and frontal sinuses share a common drainage pathway into the middle meatus via the OMU. The OMU is formed by the uncinate process and adjacent passages. The maxillary sinus drains through the maxillary ostium into the infundibulum, which joins with drainage from the anterior ethmoid air cells. The infundibulum empties into the hiatus semilunaris, which also connects with the drainage pathway of the frontal sinus, before draining into the middle meatus [Figure 2]^[2,3]. Anatomic variants of these sinuses and drainage pathways are common^[4,5].

The sphenoid sinus drains into the SER of the superior meatus before emptying into the nasal cavity [Figure 3]. Primary sphenoid sinus tumors are rare, accounting for 1%-2% of paranasal sinus tumors^[6].

The pterygopalatine fossa (PPF) is an anatomically complex space bordered by the posterior wall of the maxillary sinus anteriorly, the pterygoid bone posteriorly, the palatine bone medially, and the greater wing of the sphenoid superiorly. It communicates with the nasal cavity through the sphenoopalatine foramen. The pterygomaxillary fissure connects this space laterally with the infratemporal fossa and communicates anteriorly and superiorly with the inferior orbital fissure, which transmits the infraorbital nerve, artery, and vein. The V2 segment of the trigeminal nerve traverses the cavernous sinus and enters the PPF through the foramen rotundum, while the vidian nerve and artery pass through the vidian canal [Figures 4 and 5]^[7,8]. All these structures may be compressed or invaded by sinonasal tumors. A thorough understanding of these anatomic relationships is essential for accurate tumor mapping and surgical planning to minimize complications.

CT and MR approach to sinonasal tumors

The initial symptoms of sinonasal neoplasms include nasal obstruction, sinus pain, epistaxis, headache, proptosis, visual changes, and ophthalmoplegia^[9]. Endoscopy allows visualization of only the superficial portions of the tumor, while imaging enables assessment of the full submucosal extent^[9]. In many cases, a specific diagnosis based on imaging alone is not possible due to limited specificity and significant overlap in the imaging appearances of different tumors on CT and magnetic resonance (MR)^[10]. The primary goals of

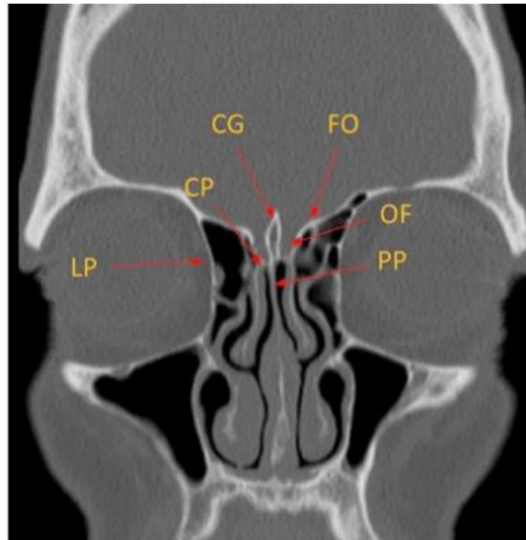


Figure 1. Coronal CT image depicting the key anatomy of the ethmoid bone. CG: Crista galli; FO: fovea ethmoidalis; CP: cribriform plate; OF: olfactory fossa; LP: lamina papyracea; PP: perpendicular plate of the ethmoid bone; CT: computed tomography.

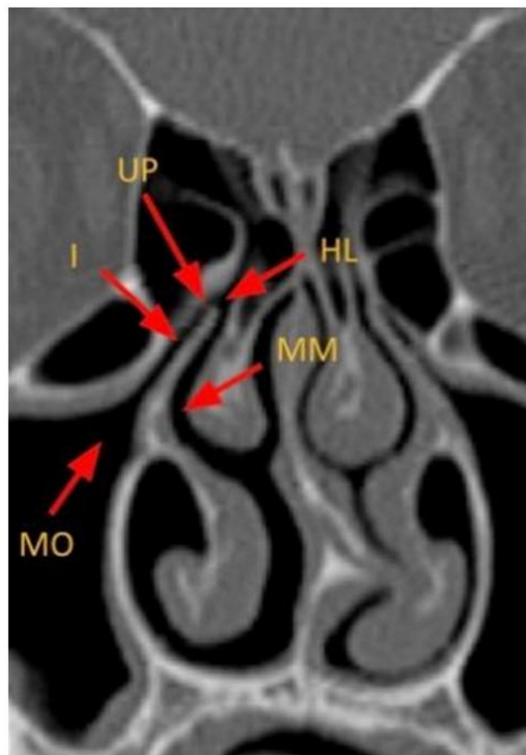


Figure 2. Coronal CT image depicting the key anatomy of the anterior OMU. MO: Maxillary ostium; I: infundibulum; HL: hiatus semilunaris; MM: middle meatus; UP: uncinate process; CT: computed tomography; OMU: ostiomeatal unit.

imaging are to distinguish inflammatory from neoplastic disease and to determine the nature and extent of the tumor (tumor mapping). The highest diagnostic accuracy is achieved using both CT and MR^[9,11].

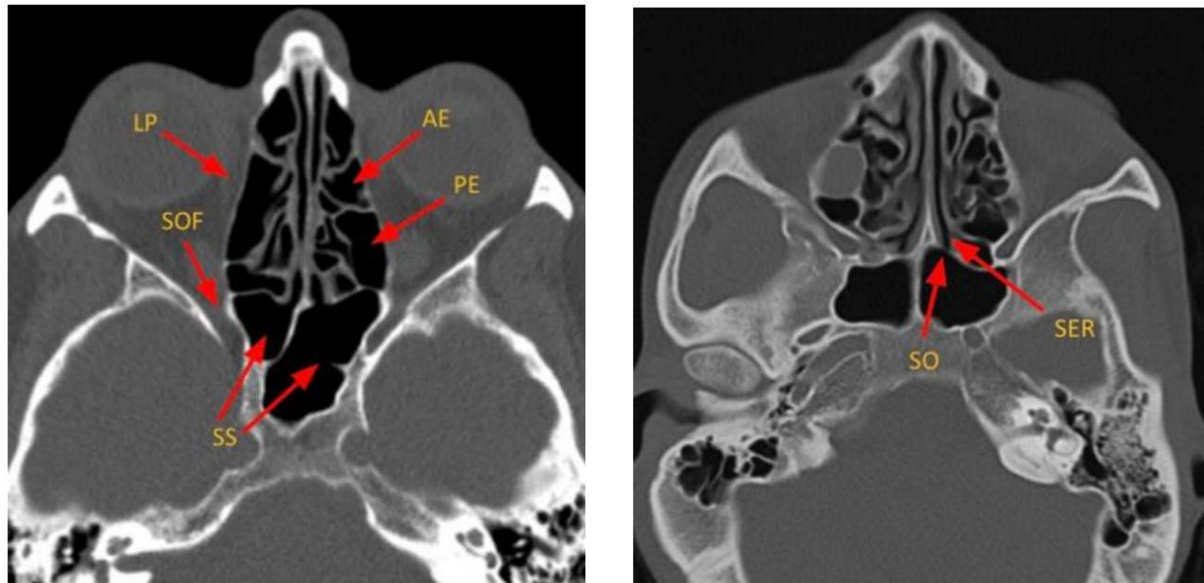


Figure 3. Axial CT images depicting the key components of ethmoid air cells and sphenoid sinuses. LP: Lamina papyracea; SOF: superior orbital fissure; SS: sphenoid sinus; SER: sphenothethmoidal recess; SO: sphenoid ostium; AE: anterior ethmoid air cells; PE: posterior ethmoid air cells; CT: computed tomography.

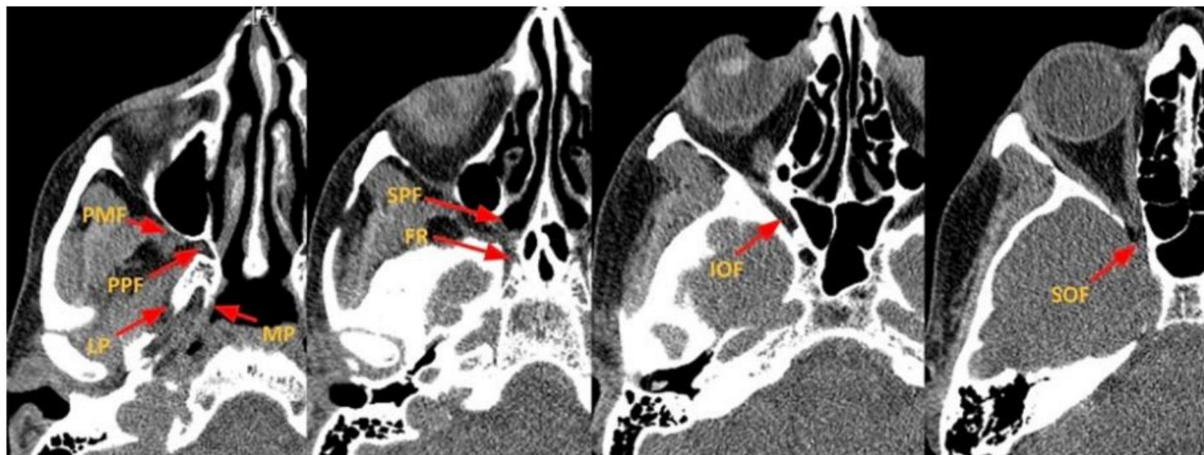


Figure 4. Axial CT images depicting the key components of the PPF and skull base foramina. PPF: Pterygopalatine fossa; PMF: pterygomaxillary fissure; LP: lateral plate of the pterygoid; MP: medial plate of the pterygoid; SPF: sphenopalatine foramen; FR: foramen Rotundum; IOF: inferior orbital fissure; SOF: superior orbital fissure; CT: computed tomography.

Paranasal CT is typically performed first in cases of acute recurrent or chronic rhinosinusitis^[12]. Radiological features suggestive of malignancy include unilateral sinus disease, bony involvement, extensive soft-tissue mass, tumor necrosis, and lymphadenopathy (LAD)^[12]. Four important patterns of bony involvement have been described^[12]: Bony destruction/erosion is aggressive and suspicious for malignancy, but may also be seen with osteomyelitis, invasive fungal sinusitis, or granulomatous disease^[12]. Bony remodeling, deficiency, or dehiscence is associated with long-standing processes such as mucocoele, polyp, inverted papilloma (IP), slow-growing neoplasms (e.g., schwannoma), or cephaloceles [Figure 6]^[12]. Reactive sclerosis is usually a sequela of chronic infection^[12]. New bone formation may occur with chondrosarcoma and osteosarcoma [Figure 7]^[12].

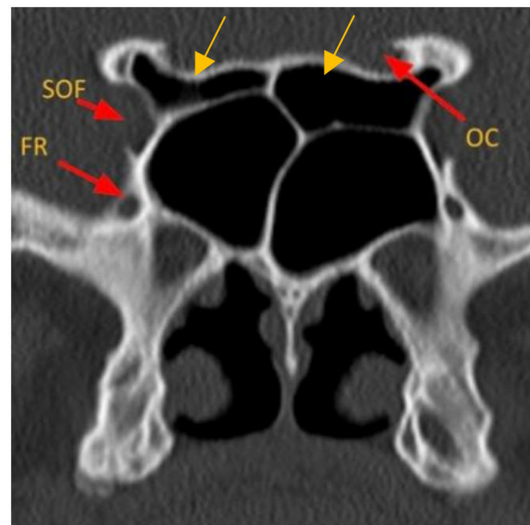


Figure 5. Coronal CT image of skull base foramina. SOF: Superior orbital fissure; FR: foramen rotundum; OC: optic canal. Onodi air cells (yellow arrows), anatomical variant. CT: Computed tomography.

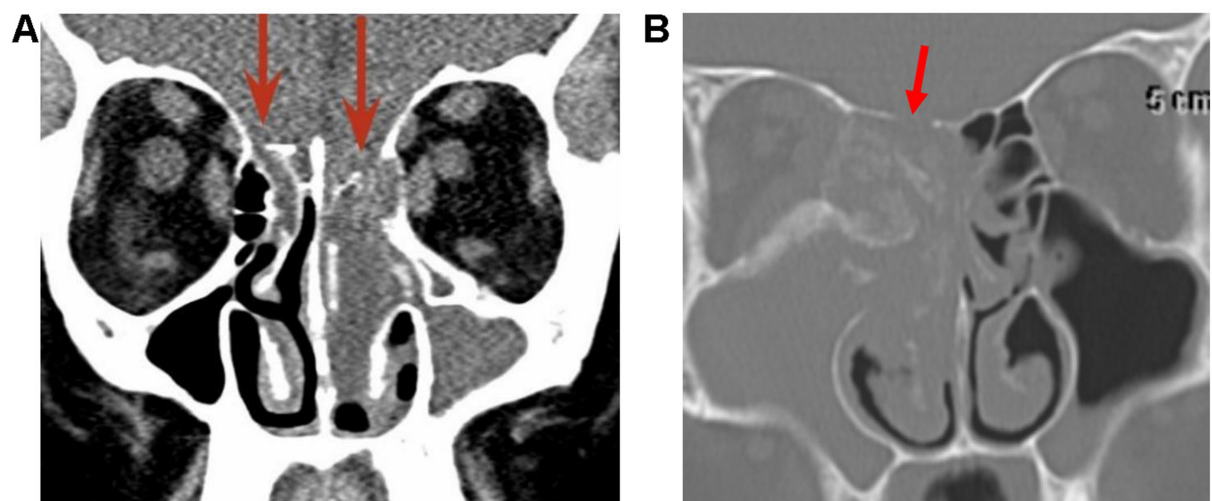


Figure 6. Arrows point to long-standing bony deficiency/dehiscence associated with a cephalocele (A) and bony destruction/erosion associated with a malignant NUT carcinoma (B). NUT: Nuclear protein of the testis.

Osteomas are the most common benign sinonasal tumors and are usually incidental findings^[13]. They occur most frequently in the frontal sinus and typically require no treatment unless they enlarge significantly or obstruct drainage pathways^[13]. On CT, osteomas may show dense cortical bone or a ground-glass appearance, making them difficult to distinguish from fibrous dysplasia [Figure 8]^[13]. Fibrous dysplasia is characterized by a ground-glass appearance on CT. MR imaging can be variable, depending on the relative amount of cystic components and fibrous tissue, and may show mild post-contrast enhancement [Figure 9]^[13]. The radiologic diagnosis of fibrous dysplasia relies primarily on CT.

Compared with CT, MR offers multiplanar imaging capabilities and superior soft-tissue contrast, which aids in differentiating tumors from trapped secretions [Figure 10]^[10]. Secretions, which have high water content, typically demonstrate high T2 signal and peripheral contrast enhancement^[10]. Most sinonasal tumors are

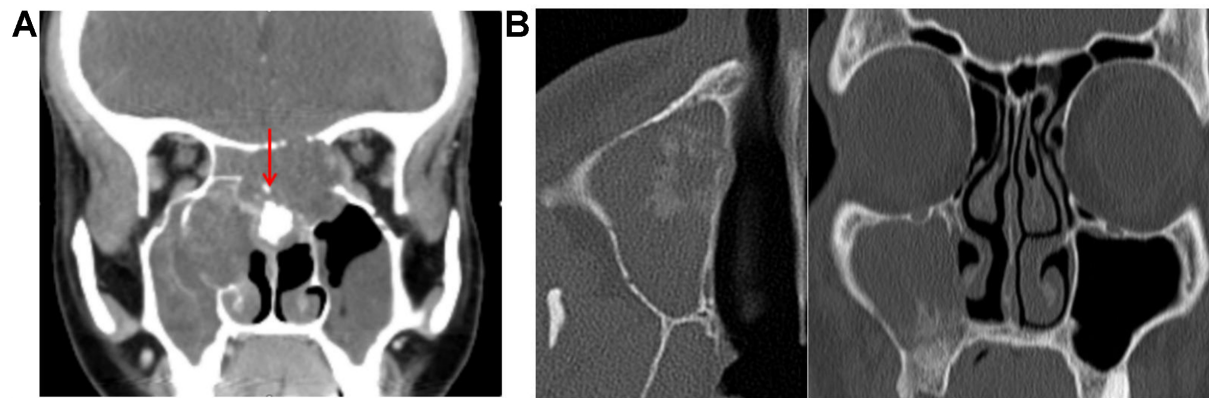


Figure 7. (A) Coronal CT showing the characteristic “ring and arc” appearance of a chondroid matrix in chondrosarcoma; (B) CT demonstrating “sunburst” periostitis and osteoid matrix typical of osteosarcoma. CT: Computed tomography.

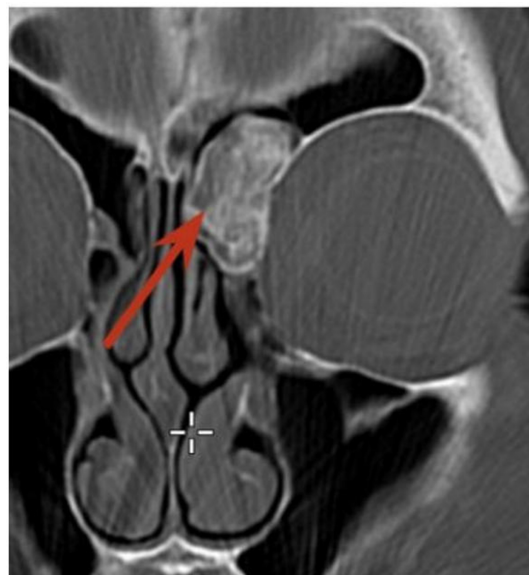


Figure 8. Red arrow points to an osteoma in the left frontal sinus.

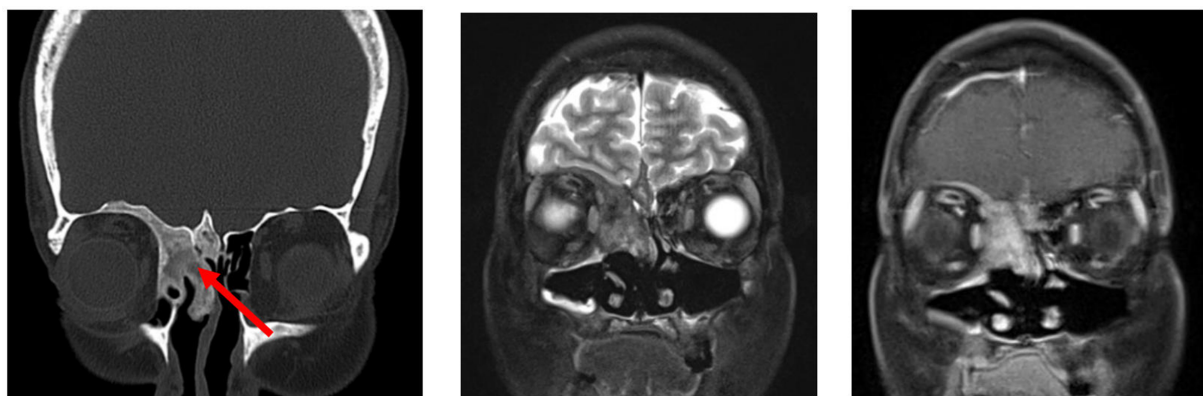


Figure 9. Coronal CT and MR images (left to right: T2 and post-contrast T1) of fibrous dysplasia showing the characteristic ground-glass matrix on CT (arrow). CT: Computed tomography; MR: magnetic resonance.

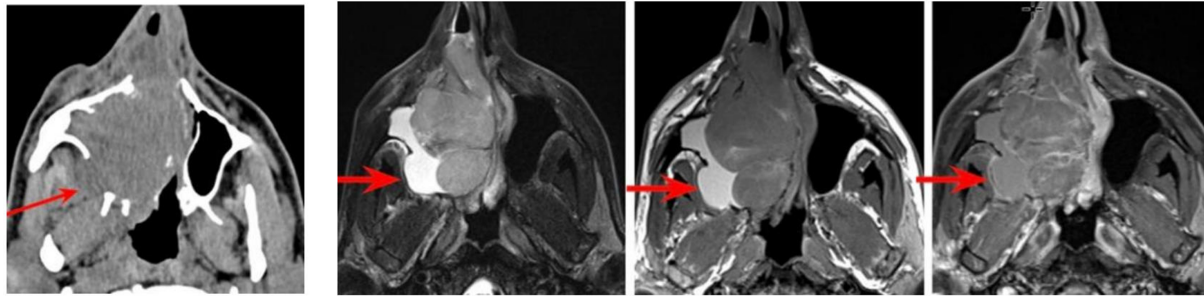


Figure 10. CT and MR images of right nasal melanoma. On CT, tumor and trapped secretions are difficult to differentiate, whereas MRI distinguishes tumor from T1 and T2 hyperintense secretions in the posterior lateral maxillary sinus antrum (arrows). CT: Computed tomography; MR: magnetic resonance; MRI: magnetic resonance imaging.

highly cellular, with intermediate-to-low signal intensity on T2-weighted images and solid enhancement, except for vascularized polyps, which can also demonstrate solid enhancement [Figures 11 and 12]^[10]. Hypercellular tumors may also show restricted diffusion on diffusion-weighted imaging.

Cross-sectional imaging should be carefully reviewed for evidence of tumor extension, including direct invasion, perineural spread, or metastatic spread^[13]. Tumors originating in the maxillary antrum may extend anteriorly, into the retromaxillary space, or inferiorly into the hard palate. The PPF is a critical site to evaluate^[10]. From the PPF, tumors can spread into the orbit, infratemporal fossa, and intracranial compartment^[10]. They may also extend via the pterygomaxillary fissure into the masticator space^[10] or via the inferior orbital fissure into the orbital apex. Involvement of the foramen rotundum can lead to spread into the middle cranial fossa^[10,11]. Tumors can also extend superiorly through the cribriform plate into the anterior cranial fossa (ACF)^[11]. Eisen *et al.* reported that preoperative MR can accurately predict dural invasion when pial enhancement (82%), nodular enhancement (95%), or dural enhancement > 5 mm thick (91%) is present^[14]. In contrast, linear dural enhancement does not necessarily indicate tumor infiltration^[14]. A prospective blinded MRI study of 50 sinonasal and anterior skull-base tumors found that dural thickening > 2 mm, loss of the hypointense zone, and nodular dural enhancement were highly predictive of dural invasion [Figure 13]^[15].

Regarding orbital involvement, bony erosion alone is not an indication for orbital exenteration. Instead, breach of the periosteum is an important finding to report^[11]. MRI has a higher negative predictive value than positive predictive value; therefore, suspected invasion should be confirmed histologically during surgery^[11,16]. The periosteum appears hypointense on all MRI sequences, and this low-signal boundary remains visible despite bony erosion if the periorbita is intact. Loss of this low-signal boundary indicates periorbital invasion [Figure 14]^[11,17]. Eisen *et al.* evaluated ten preoperative imaging criteria for orbital invasion^[18]. All MRI cases showing extraocular muscle enlargement, signal change, or enhancement had pathologically confirmed invasion (PPV = 100%)^[18]. Orbital fat invasion demonstrated PPVs of 80% on MRI and 86% on CT^[18]. However, no single criterion exceeded 79% overall predictive accuracy for orbital invasion^[18].

Overview of sinonasal tract tumors

Although sinonasal tract tumors can share overlapping imaging features, a comprehensive, pattern-based approach can help narrow the differential diagnosis before tissue confirmation. Key considerations include identifying the tumor's site of origin, assessing local disease behavior, and recognizing common and uncommon CT and MR imaging characteristics of sinonasal neoplasms, while taking into account the patient's demographics, risk factors, and clinical presentation. For example, bilateral involvement is

↑ T2, Peripheral Gd +	↓ T2, Solid Gd +
Retention cyst -Submucosal Mucinous/Serous gland collection -Partially aerated sinus	Neoplasm
Polyp -Fluid deep to the lamina propria -Mass effect	
Mucocele -Trapped secretion in the obstructed sinus -Airless Expanded sinus	

Figure 11. MRI tissue characterization. MRI: Magnetic resonance imaging.

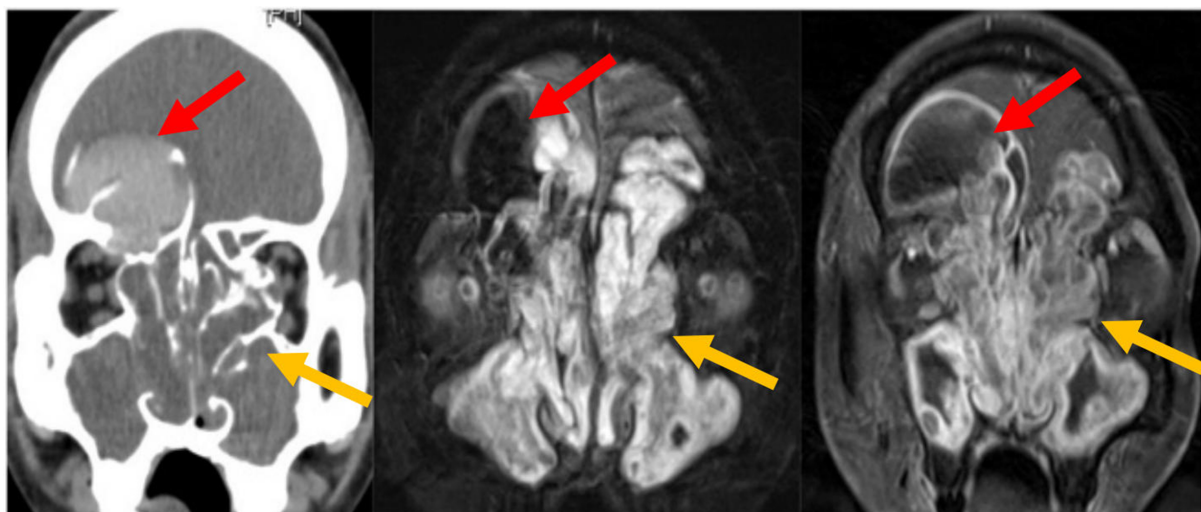


Figure 12. Coronal CT and MRI images of a right frontal sinus mucocoele and sinonasal polyposis. The right frontal sinus is airless and expanded. Hyperdense secretions on CT correspond to the signal void on MRI (red arrows). Bony deficiency surrounds the mucocoele. Polyps show low CT attenuation and characteristic T2 hyperintensity with peripheral enhancement on MR (yellow arrows). CT: Computed tomography; MRI: magnetic resonance imaging; MR: magnetic resonance.

typically observed in benign conditions such as sinonasal polyposis [Figure 12] and respiratory epithelial adenomatoid hamartoma (REAH) [Figure 15]. In contrast, unilateral isolated lesions warrant thorough evaluation for neoplasms, such as carcinoma or inverting papilloma obstructing a sinus drainage pathway [Figures 10, 13 and 14]. Papilloma is the most common benign sinonasal tumor, whereas SCC is the most frequent malignancy. The maxillary antrum is the most common site of malignancy; however, adenocarcinomas are more likely to arise in the ethmoid sinuses^[19]. Adenoid cystic carcinoma (AdCC) shows a predilection for perineural spread, while chondrosarcoma and osteosarcoma exhibit characteristic chondroid and osteoid tumor matrices, respectively, on CT and MR imaging. Esthesioneuroblastoma (ENB) commonly arises in the nasal vault, melanomas are frequently found in the nasal cavity, and sinonasal undifferentiated carcinoma (SNUC) and sinonasal neuroendocrine carcinoma (SNEC) represent aggressive tumors of the nasal and ethmoidal regions. An International Consensus Statement on Sinonasal Tumors was released in February 2024, and the following section highlights commonly encountered sinonasal tract

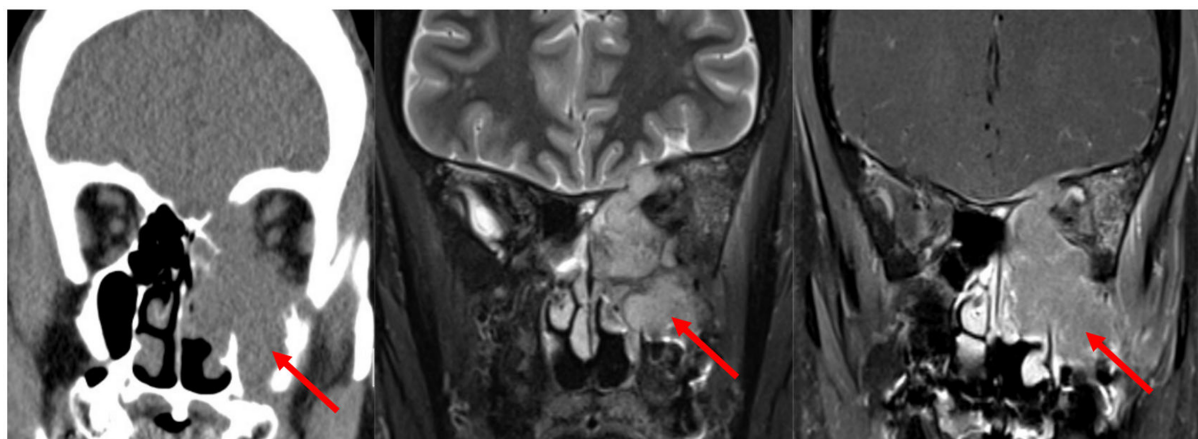


Figure 13. SCC with dural invasion of the left ACF. Findings include bony erosion, loss of the hypointense zone, and nodular dural enhancement (arrows). SCC: Squamous cell carcinoma; ACF: anterior cranial fossa.

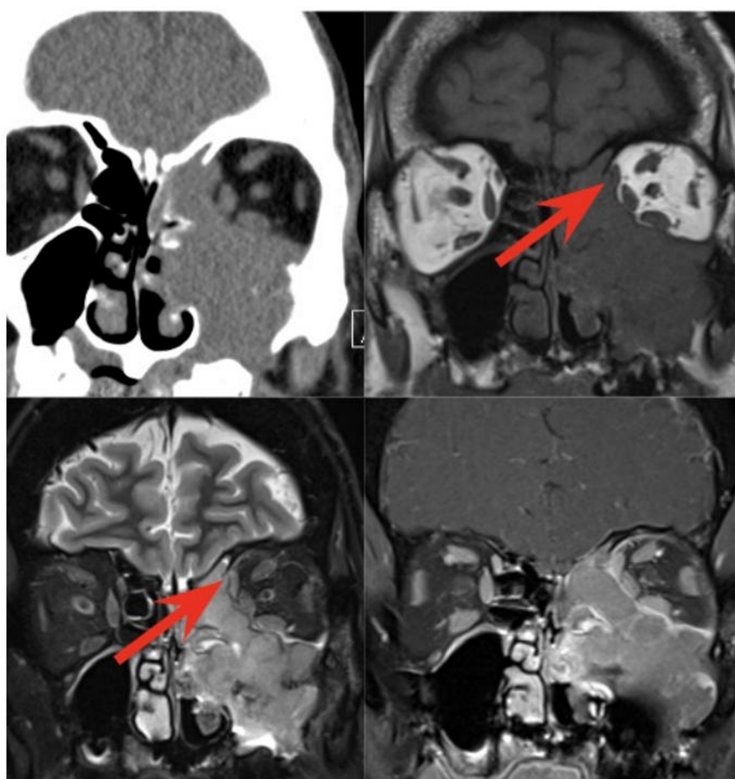


Figure 14. SCC with orbital invasion. Arrows indicate loss of the well-defined low-signal boundary, consistent with periorbital infiltration. SCC: Squamous cell carcinoma.

tumors, organized according to the statement, starting with benign lesions followed by malignant ones^[20].

HAMARTOMAS

The most common types of sinonasal hamartomas are REAH and seromucinous hamartoma (SMH).

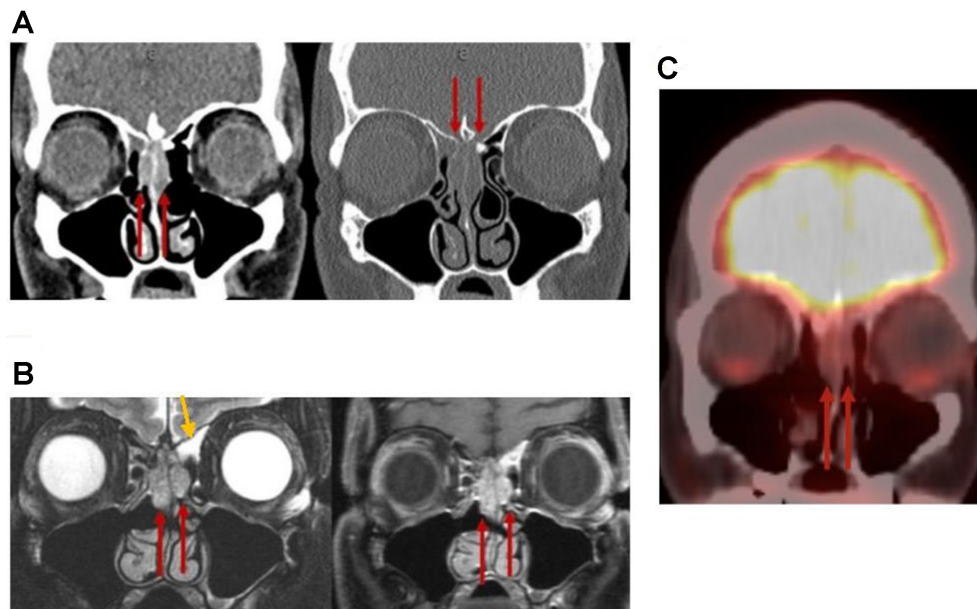


Figure 15. REAH. (A) Coronal CT and (B) coronal MRI images [T2 (left) and postcontrast T1 (right)] demonstrate widening of the bilateral OCs (red arrows) and trapped secretions in the left frontoethmoidal recess (yellow arrow); (C) Coronal F-18 FDG PET shows no FDG-avid signal in this region. REAH: Respiratory epithelial adenomatoid hamartoma; CT: computed tomography; MRI: magnetic resonance imaging; OCs: olfactory clefts.

REAH and SMH are benign polypoid lesions that share overlapping symptoms and imaging features. REAH most commonly arises in the olfactory clefts (OCs), but it can also occur less frequently in the septum, middle turbinate, and ostiomeatal complex. It often presents bilaterally, and its presence is suspected when the combined OC width on coronal CT exceeds 1.0 cm at the widest point [Figure 15]^[21]. SMH, by contrast, typically presents as a unilateral polypoid mass originating from the posterior nasal septum^[22]. The MRI features of both lesions remain poorly characterized in the literature due to their rarity.

SINONASAL PAPILLOMA

Sinonasal papillomas comprise different histologic subtypes, the most common being IP, a non-cancerous epithelial tumor with a risk of malignant transformation. On CT, soft-tissue attenuation is typically observed in the nasal cavity, often arising from the middle turbinate, and is frequently associated with bony erosion and remodeling^[23]. Focal hyperostosis at the tumor origin and intralesional calcifications are additional features that may suggest the presence of IP^[23]. A characteristic imaging feature of IP is the convoluted cerebriform pattern (CCP), defined as alternating linear or curvilinear hypointense and hyperintense signals, which can appear either diffusely or focally within the tumor^[24]. CCP is identifiable on both T2-weighted and post-contrast T1-weighted MRI sequences [Figure 16]. However, CCP is not specific to IP and may also be seen in malignant cancers such as SCC and AdCCs^[24]. Concomitant SCC in IP should be suspected when there is focal loss of CCP, intratumoral necrosis, aggressive bony erosion, or extra-sinonasal extension^[24]. When a lesion demonstrates CCP along with T1 hyperintensity, oncocytic papilloma - which carries a lower malignant potential - should also be considered in the differential diagnosis^[25].

JUVENILE NASOPHARYNGEAL ANGIOFIBROMA

Juvenile nasopharyngeal angiofibroma (JNA) is a rare, benign but locally aggressive, highly vascular tumor that accounts for 0.05% of all head and neck tumors^[16,26]. It occurs predominantly in adolescent males^[16,27].

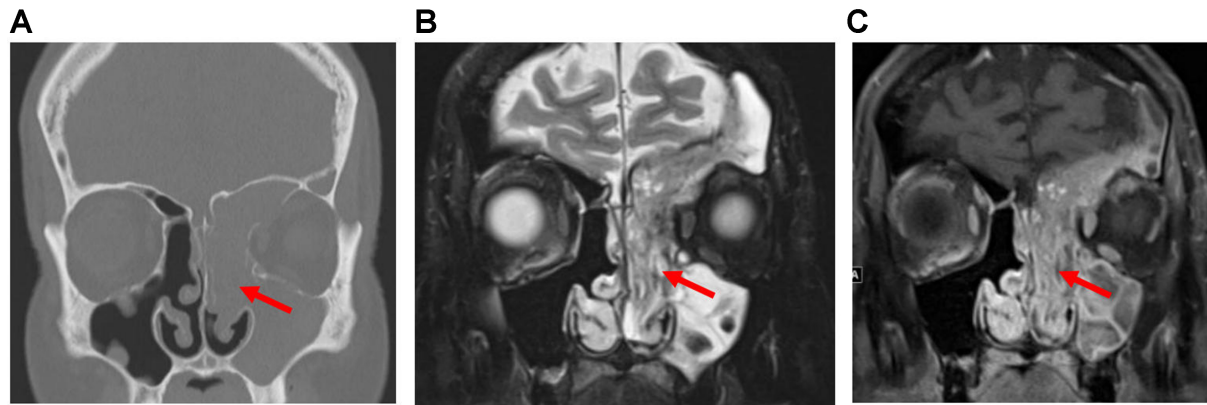


Figure 16. Sinonasal papilloma. (A) Coronal CT image of the sinonasal region in a patient with IP showing an expansile lesion with soft-tissue attenuation in the left nasal cavity, maxillary sinus, frontal sinus, and ethmoid sinus (arrow). Bony remodeling and dehiscence of the nasal cavity and sinus walls, as well as erosion of the ethmoid septa, are also evident; (B and C) Coronal T2-weighted and post-contrast T1-weighted MRI images of the same patient demonstrate CCP, visible as alternating curvilinear hypointense and hyperintense signals diffusely within the tumor (arrows). CT: Computed tomography; IP: inverted papilloma; MRI: magnetic resonance imaging; CCP: convoluted cerebriform pattern.

The exact origin site of JNA remains uncertain, but it is thought to arise from the PPF or pterygoid canal. JNAs can expand in multiple directions, extending into the nasal cavity, nasopharynx, orbital apex, and intracranially into the middle cranial fossa. Bone changes typically involve remodeling and erosions, most often at the level of the pterygoid root^[16]. On CT and MR, key diagnostic features include identification of the site of origin, intense hypervascular enhancement on post-contrast images, and the tumor's growth pattern into adjacent structures, which together enable accurate imaging diagnosis [Figure 17]^[26]. Additionally, multiple signal flow voids within the lesion on both T1- and T2-weighted sequences—corresponding to large intralesional vessels—are often characteristic^[26]. Typical JNAs can be diagnosed with high confidence using CT and MR, and preoperative biopsy is generally avoided due to the risk of severe hemorrhage^[16].

AMELOBLASTOMA

Ameloblastoma is a benign but locally aggressive, slow-growing tumor, ranking as the second most common benign odontogenic tumor after odontoma^[27]. It typically presents in middle age as a hard, painless mass and often arises in the mandible (80%), particularly near the angle, or in the maxilla (20%), commonly in the third molar region^[16,27]. Maxillary ameloblastomas frequently extend into the maxillary sinus. Although benign, these tumors are associated with a high recurrence rate^[16]. When large, they can erode through the bony cortex into adjacent soft tissues^[27]. Despite their histologically benign classification, metastases from ameloblastomas have been reported in extremely rare cases. According to the World Health Organization (WHO), malignant ameloblastoma is defined as a histologically benign-appearing ameloblastoma that has metastasized, most commonly to the lungs^[27]. Importantly, the metastatic nodules retain the benign histological features of the primary tumor^[27].

On CT imaging, ameloblastomas typically appear as multiloculated, expansile, solid-and-cystic non-enhancing “soap-bubble” lesions with a thin, well-defined border^[16]. On MRI, they demonstrate a mixed solid and cystic appearance with thickened walls and avid contrast enhancement of the solid components [Figure 18]^[16,27].

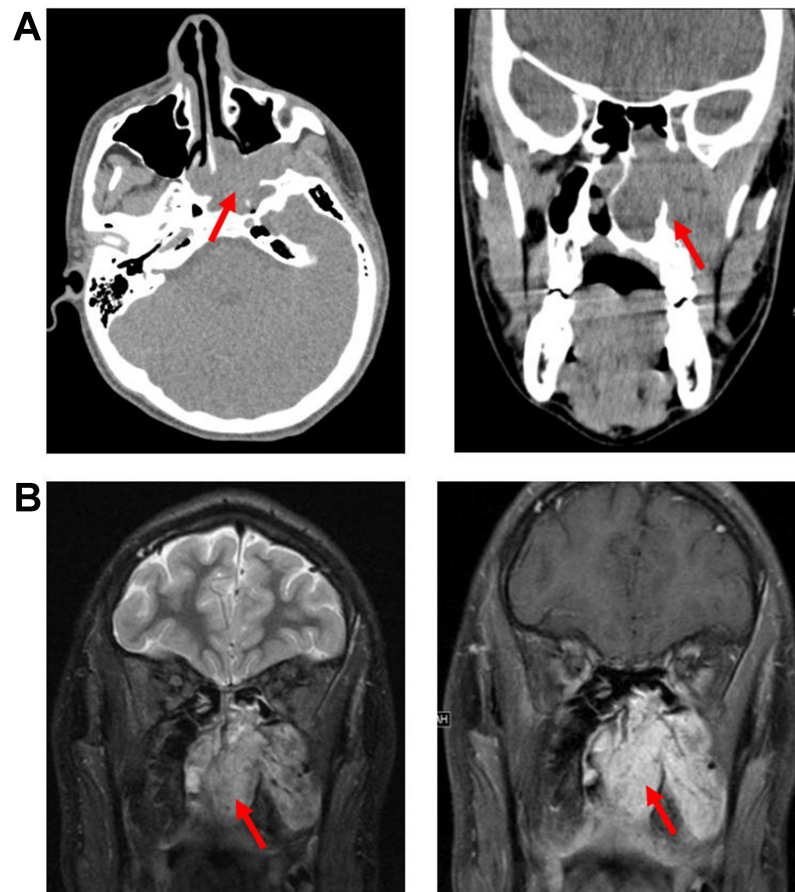


Figure 17. JNA. (A) Axial (left) and coronal (right) non-contrast CT images, and (B) coronal T2-weighted (left) and post-contrast T1-weighted (right) MRI images, demonstrate an expansile, hyperenhancing mass arising from the left PPF and extending into the left nasal cavity (arrows). JNA: Juvenile nasopharyngeal angiofibroma; CT: computed tomography; MRI: magnetic resonance imaging; PPF: pterygopalatine fossa.

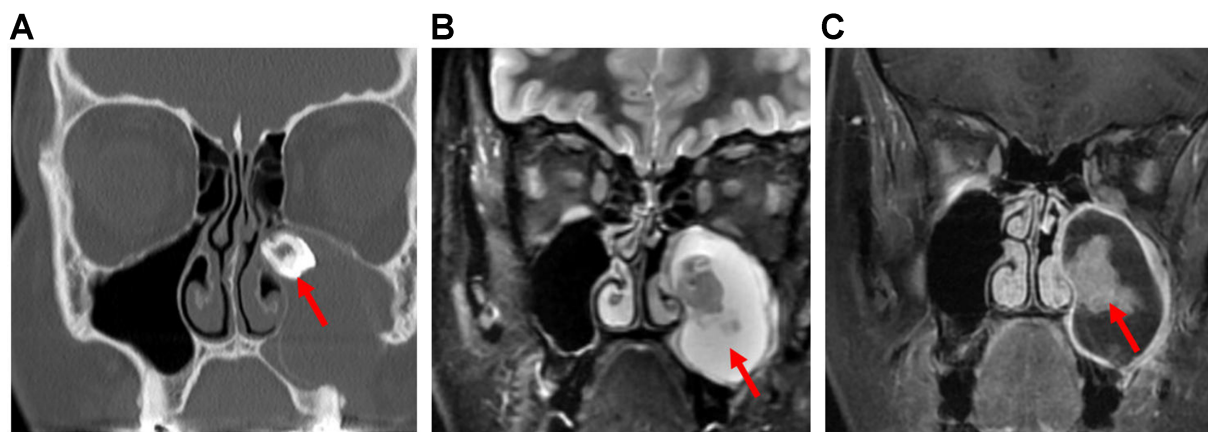


Figure 18. Ameloblastoma. (A) Coronal non-contrast CT image, (B) Coronal T2-weighted MRI, and (C) coronal post-contrast T1-weighted MRI show an expansile cystic mass (arrow, B) involving the left maxillary alveolus and extending into the left maxillary sinus. Avid enhancement of the internal solid component (arrow, C) is evident on the post-contrast MRI. The lesion is also associated with an unerupted tooth (arrow, A). CT: Computed tomography; MRI: magnetic resonance imaging.

SINONASAL SQUAMOUS CELL CARCINOMA

Sinonasal squamous cell carcinomas (SNSCCs) account for 61% of all sinonasal malignancies. The maxillary antrum is the most common site of origin, followed by the nasal cavity and ethmoid air cells^[28]. SNSCCs are classified into keratinizing and non-keratinizing subtypes, which share overlapping imaging features but differ slightly in their preferred locations. Both subtypes are frequently encountered in the maxillary antrum and nasal cavity; however, keratinizing SNSCCs are more likely to arise in the nasal vestibule^[25]. Non-keratinizing SNSCCs are associated with HPV type 16, which is linked to higher incidence and improved overall survival^[25,28]. A newly recognized subtype of non-keratinizing SNSCCs, DEK-AFF2-rearranged carcinoma, demonstrates a predilection for the posterior portion of the middle turbinate^[25].

The imaging features of SNSCCs reflect their aggressive biological behavior, typically showing bone destruction and extensive locoregional invasion, including perineural spread as well as orbital and intracranial extension^[29]. CT and contrast-enhanced MRI are essential for evaluating osseous involvement and for comprehensive tumor mapping^[28]. On MRI, lesions often demonstrate intermediate signal intensity on both T1- and T2-weighted sequences and reduced ADC values [Figure 19]^[28,29]. If the tumor spreads to regions with rich lymphatic drainage, such as the nasopharynx or hard palate, it can metastasize to the cervical chain and lateral retropharyngeal lymph nodes^[30].

HPV-related multiphenotypic sinonasal carcinoma is a recently recognized entity included in the 2022 WHO classification of head and neck cancers. It demonstrates a propensity for the nasal cavity, particularly the turbinates^[25]. This tumor is linked to high-risk HPV type 33 and is distinct from HPV-positive SNSCCs. Unlike other HPV-related head and neck carcinomas, it has not been reported to present with cystic nodal metastasis^[31].

SINONASAL ADENOCARCINOMA

Sinonasal adenocarcinoma (SNAC) is a rare malignancy of the sinonasal tract that arises from the respiratory surface epithelium or the underlying seromucinous glands. These tumors are classified into salivary-type and non-salivary-type^[32]. Histologically, salivary-type SNAC resembles tumors arising in the salivary glands and accounts for 5%-10% of all SNACs^[32]. Tumor subtypes include AdCC, myoepithelial carcinoma, and acinic cell carcinoma. Among these, AdCC is the most common salivary-type SNAC and represents the second most common sinonasal malignancy overall, after SCC^[32]. AdCC typically occurs in the maxillary antrum or nasal cavity and is associated with a poor long-term prognosis due to local invasion and perineural spread [Figure 20]^[16,32].

Non-salivary-type SNACs are subdivided into intestinal and non-intestinal types. Intestinal-type SNACs, the second most common form of SNAC^[32], histologically resemble carcinomas of intestinal origin. These aggressive tumors most frequently arise in the ethmoid air cells, followed by the nasal cavity and maxillary antrum^[32]. At diagnosis, they commonly show local extension into the orbit, PPF, and cranial cavity^[16].

Non-intestinal-type SNACs are distinct from both salivary and intestinal types in terms of histology. These rare, heterogeneous tumors display diverse morphological patterns, commonly occur in the ethmoid air cells and nasal cavity, and are associated with poor prognoses^[32].

MR imaging of SNAC is primarily used for tumor mapping and assessment of submucosal involvement, local invasion, perineural spread, and bone infiltration. However, the signal characteristics on both CT and MR images are often nonspecific and generally do not enable reliable differentiation of SNAC from other sinonasal malignancies^[16].

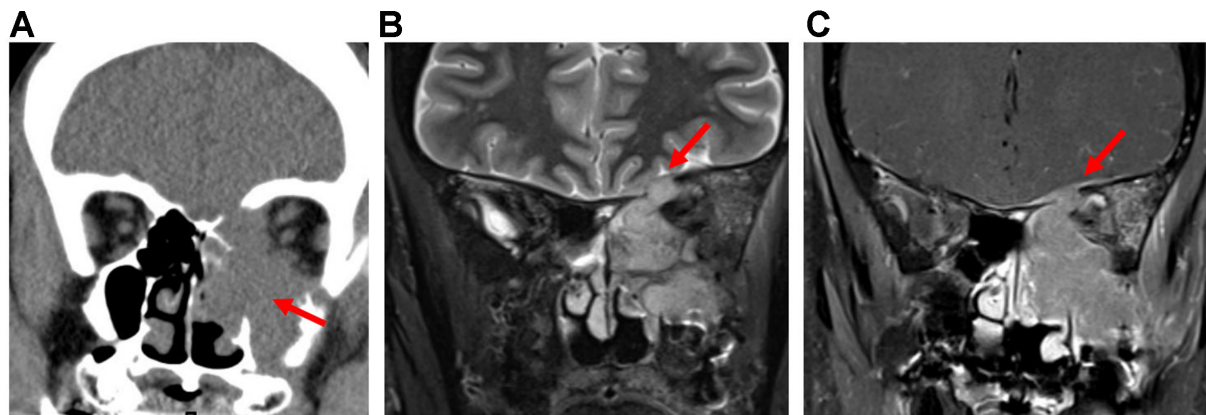


Figure 19. SNSCC. (A) Coronal CT image of the sinonasal cavity shows a destructive soft-tissue mass centered in the left maxillary antrum with erosion of the sinus wall, nasal cavity, ethmoid complex, orbit, and anterior skull base (arrow); (B) Coronal T2-weighted MRI demonstrates intermediate signal intensity of the tumor and loss of the hypointense zone, indicating dural invasion (arrow); (C) Coronal post-contrast T1-weighted MRI shows nodular tumor extension through the anterior skull base defect with hyperenhancing thickening of the overlying dura (arrow). SNSCC: Sinonasal squamous cell carcinoma; CT: computed tomography; MRI: magnetic resonance imaging.

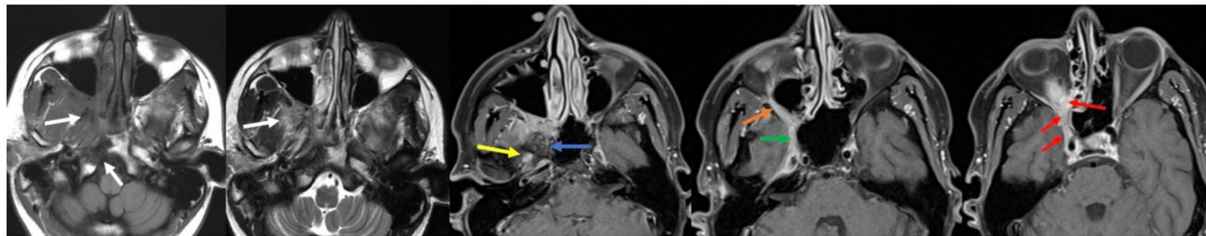


Figure 20. AdCC. From left to right: axial precontrast T1, axial T2, and three axial post-contrast T1 images. AdCC demonstrates invasion of the right skull base with sclerosis of the pterygoid and sphenoid bones (white), and perineural invasion involving the PPF, Vidian canal (blue), foramen ovale (yellow), foramen rotundum (green), inferior orbital fissure (orange), superior orbital fissure (red), orbital apex (red), and ventral cavernous sinus (red). AdCC: Adenoid cystic carcinoma; PPF: pterygopalatine fossa.

CHONDROSARCOMA

Chondrosarcoma is a malignant cartilaginous tumor commonly arising in the long bones and pelvis^[16]. Approximately 10% occur in the head and neck, with the maxillary sinus being the most frequent site of involvement^[16,33]. The peak incidence is observed between the ages of 40 and 60 years^[16,33]. These tumors are typically slow-growing and often cause deformation of surrounding structures.

On CT, chondrosarcomas usually appear as soft tissue masses with matrix calcifications and heterogeneous contrast enhancement^[16,33]. MRI typically shows low to intermediate signal intensity on T1-weighted images and high intensity on T2-weighted images in the non-calcified cartilaginous regions^[33]. Calcified areas often produce blooming artifacts. Post-contrast MRI demonstrates the characteristic “rings and arcs” enhancement pattern associated with fibrovascular tissue [Figure 21]^[16,33].

OLFACTORY NEUROBLASTOMA

Olfactory neuroblastoma, also known as ENB, is a rare neural crest-derived malignancy originating from the olfactory epithelium of the nasal cavity^[34]. Imaging plays a critical role in mapping both locoregional tumor extent and metastatic disease.

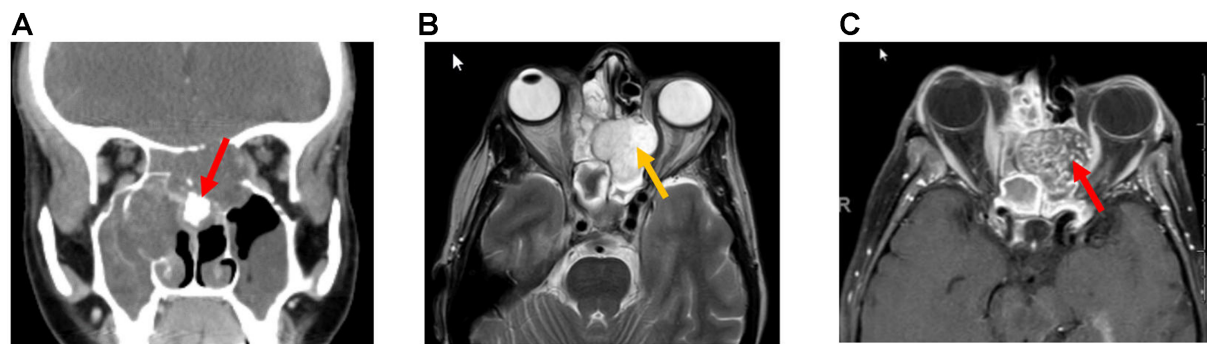


Figure 21. Sinonasal chondrosarcoma. (A) Coronal non-contrast CT demonstrates an ill-defined, low-attenuation mass expanding the nasal cavity and paranasal sinuses with osseous destruction and calcifications (arrow); (B) Axial T2-weighted MRI demonstrates the hyperintense cartilaginous matrix (yellow arrow); (C) Axial post-contrast T1-weighted MRI reveals the characteristic “rings and arcs” fibrovascular enhancement (red arrow). CT: Computed tomography; MRI: magnetic resonance imaging.

On CT, ENB typically presents as a homogeneous soft-tissue mass centered in the superior nasal cavity^[34]. Adjacent osseous structures may demonstrate either erosion or remodeling, the latter presentation being more common in tumors with indolent growth^[34]. MRI, with its superior soft-tissue resolution, is more effective in evaluating orbital involvement, intracranial extension, perineural spread, and distinguishing tumor tissue from entrapped fluid^[34,35]. MRI may also reveal cysts at the intracranial margin of the tumor, a feature highly suggestive, though not pathognomonic, of ENB^[36]. Pathology has shown these cysts to contain necrotic tumor tissue^[35]. Compared with gray matter, ENB typically appears hypointense on T1-weighted images and iso- to hyperintense on T2-weighted images, with heterogeneous post-contrast enhancement^[35].

The Kadish staging system, proposed in 1976, classifies ENB based on disease extent, underscoring the importance of imaging in the initial evaluation. In the original system, Group A includes tumors confined to the nasal cavity, Group B includes extension into the paranasal sinuses, and Group C includes invasion of the cribriform plate, skull base, intracranial cavity, or orbits [Figures 22 and 23]^[34]. In 1993, Morita *et al.* introduced Group D to highlight the frequent spread of ENB to cervical lymph nodes, most commonly level II^[37,38]. Distant metastases may involve the lungs, bones - often with spinal involvement - and the liver^[37].

SNUC

SNUC is a rare, highly aggressive, and rapidly growing malignancy^[39]. It most commonly originates in the nasal cavity or ethmoid air cells. On CT imaging, lesions are typically larger than 4 cm and demonstrate osseous destruction with aggressive locoregional invasion at the time of presentation^[40]. On MRI, tumors are usually isointense to muscle on T1-weighted sequences and hyperintense on T2-weighted sequences^[40]. Following intravenous contrast administration, lesions show heterogeneous enhancement^[40]. Because of the tumor's strong tendency for orbital and intracranial invasion as well as perineural spread, high-soft tissue resolution MRI is essential for accurate tumor mapping [Figure 24]^[40]. SNUC frequently presents with cervical nodal involvement and distant metastases, particularly to the bones and liver^[39].

NUCLEAR PROTEIN OF THE TESTIS CARCINOMA

Nuclear protein of the testis (NUT) carcinoma is an aggressive subtype of SCC that most commonly arises in the thorax, head, and neck. Its imaging features reflect its aggressive nature, typically presenting as an expansile, necrotic tumor with local invasion and possible cervical LAD^[41].

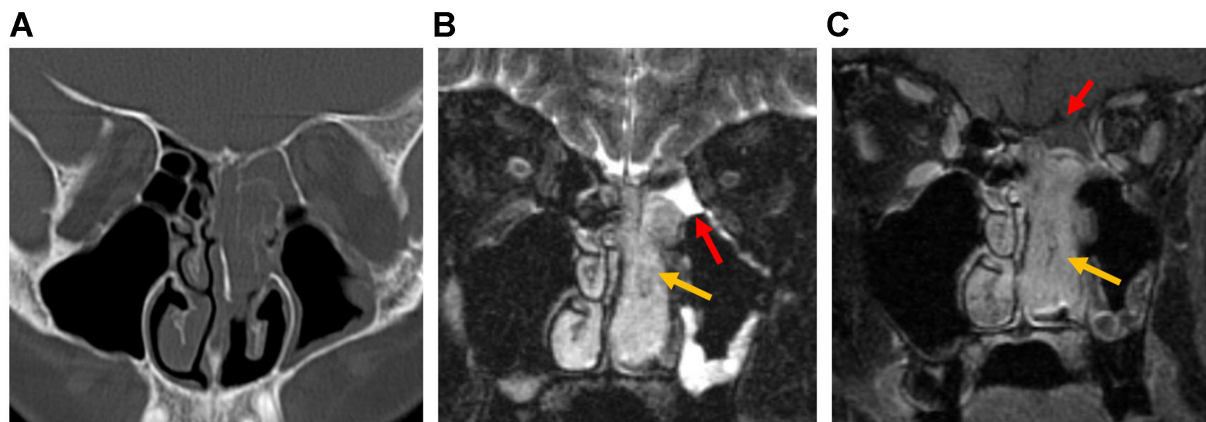


Figure 22. ENB, Kadish Group B (nasal cavity and paranasal sinus involvement). (A) Coronal CT shows soft-tissue attenuation in the left superior nasal cavity and ethmoid sinus; (B) Coronal T2-weighted MRI shows a mildly hyperintense tumor in the left nasal cavity and ethmoid sinus. Peripheral entrapped fluid (red arrow) shows marked hyperintensity compared with the tumor (yellow arrow); (C) Post-contrast T1-weighted MRI demonstrates relatively homogeneous solid enhancement of the tumor (yellow arrow), whereas the entrapped fluid shows only peripheral enhancement (red arrow). ENB: Esthesioneuroblastoma; CT: computed tomography; MRI: magnetic resonance imaging.

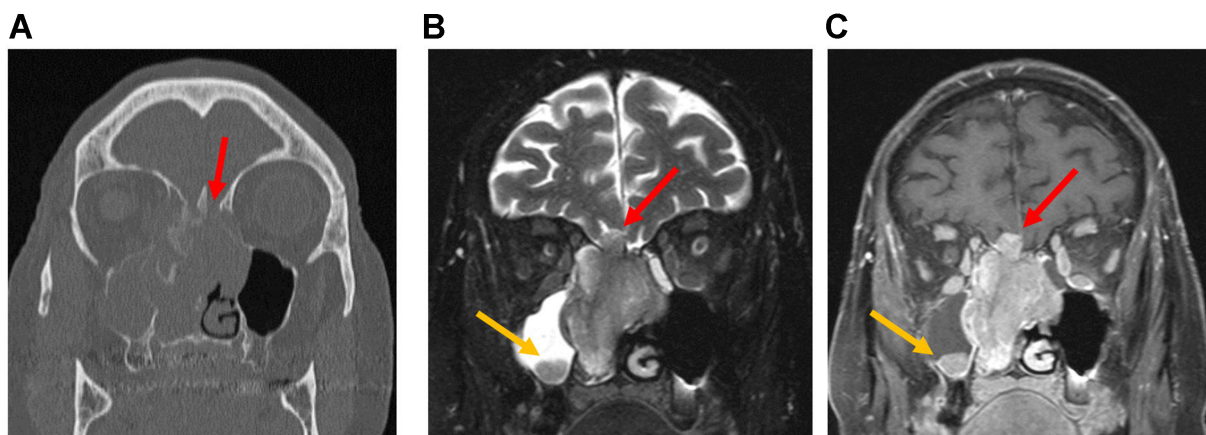


Figure 23. ENB, Kadish Group C (extension beyond nasal cavity and paranasal sinuses). (A) Coronal CT shows soft-tissue attenuation in the bilateral nasal cavities and ethmoid sinuses, with dehiscence of the cribriform plate (red arrow); (B) Coronal T2-weighted MRI shows a sinonasal tumor extending intracranially through the right cribriform plate (red arrow). T2-hyperintense trapped fluid is seen in the right maxillary sinus, along with a rounded T2-hypointense lesion at the sinus floor (yellow arrow); (C) Post-contrast T1-weighted image shows relatively homogeneous solid enhancement of the sinonasal tumor, with early intracranial dural invasion (red arrow) and an enhancing satellite lesion at the floor of the right maxillary sinus (yellow arrow). ENB: Esthesioneuroblastoma; CT: computed tomography; MRI: magnetic resonance imaging.

On CT, NUT carcinoma demonstrates aggressive features such as bony erosion, hyperostosis, avid contrast enhancement, intralesional mineralization, and orbital invasion. On MRI, the tumor usually appears hypointense on T1-weighted images and hyperintense on T2-weighted images. After contrast administration, it is enhanced with a central non-enhancing area, corresponding to necrosis [Figure 25]^[41]. NUT carcinoma may develop osseous metastases, and compared with other SCC subtypes, it less frequently presents with non-necrotic cervical LAD^[41].

SWI/SNF COMPLEX-DEFICIENT SINONASAL CARCINOMAS

Previously termed SMARCB1-deficient carcinoma, Switch/Sucrose Non-Fermentable (SWI/SNF) complex-

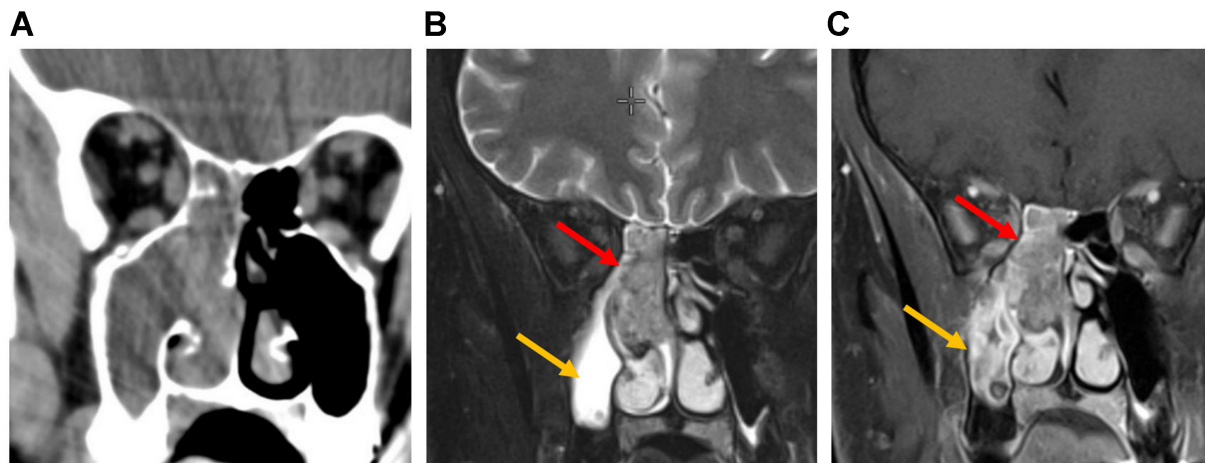


Figure 24. SNUC. (A) Coronal CT image of the paranasal sinus shows diffuse soft-tissue opacification of the right nasal cavity and ethmoid complex, with erosion of the ethmoid septa. The maxillary sinus is also opacified with lower attenuation; (B) Coronal T2-weighted MRI of the same patient shows intermediate tumor signal (red arrow). Maxillary sinus opacification appears hyperintense, consistent with retained secretions (yellow arrow); (C) Post-contrast T1-weighted MRI shows heterogeneous tumor enhancement (red arrow). The maxillary sinus demonstrates enhancing thickened mucosa, consistent with inflammatory disease (yellow arrow). SNUC: Sinonasal undifferentiated carcinoma; CT: computed tomography; MRI: magnetic resonance imaging.

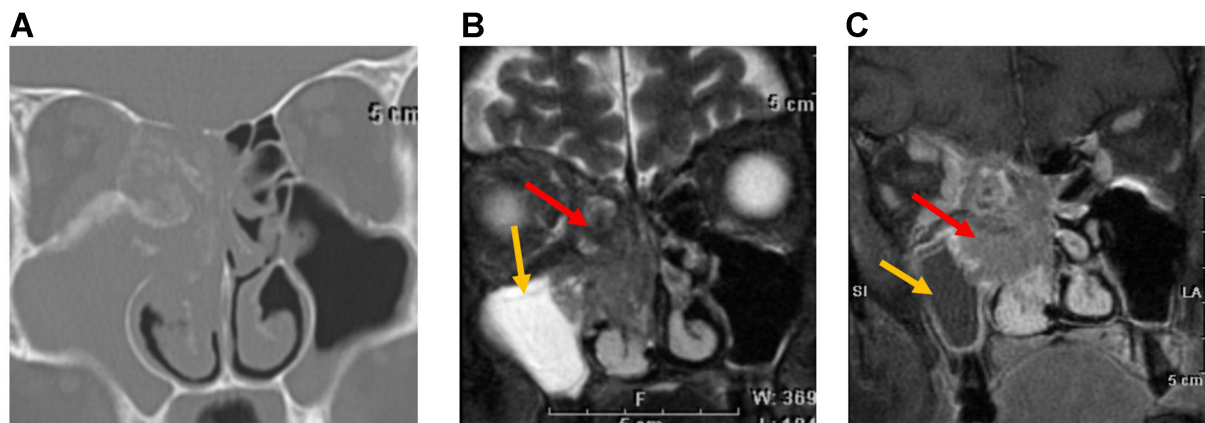


Figure 25. NUT carcinoma. (A) Coronal CT image of the paranasal sinuses in a patient with NUT carcinoma shows a lesion centered in the right nasal cavity with soft-tissue attenuation and aggressive features, including both bone erosion and hyperostosis; (B) Coronal T2-weighted image shows the tumor as isointense relative to gray matter (red arrow). The adjacent maxillary sinus exhibits a hyperintense signal consistent with trapped secretions (yellow arrow); (C) Coronal post-contrast T1-weighted image shows tumor enhancement with a central non-enhancing component reflecting necrosis (red arrow). The right maxillary sinus demonstrates peripheral enhancing mucosa, consistent with an inflammatory process and trapped secretions (yellow arrow). NUT: Nuclear protein of the testis; CT: computed tomography.

deficient sinonasal carcinoma is a newly recognized entity in the 2022 WHO classification. It is defined by the loss of the complex subunits, most commonly SMARCB1, but also SMARCA2 or SMARCA4^[25].

This highly aggressive tumor typically presents at an advanced stage, arising from the nasal cavity or nasoethmoidal region, with frequent locoregional invasion into the orbits and intracranial extension^[42]. On CT imaging, intralesional calcifications have been reported, which may represent retained bony fragments accompanied by an aggressive “hair-on-end” periosteal reaction^[42]. Compared with gray matter, these lesions typically appear isointense on T1-weighted images and show variable signal intensity on T2-

weighted images^[42]. They generally demonstrate avid contrast enhancement and moderately restricted diffusion [Figure 26]^[42].

SNEC

SNEC is a rare, highly aggressive malignancy with a high risk of recurrence. It shares a common site of origin with SNUC, particularly in the ethmoid sinuses^[43]. SNEC most commonly occurs in patients in their fifth or sixth decade of life^[44].

On CT, the tumors may appear isodense or mildly hyperdense and typically show avid contrast enhancement. On MRI, they usually present with ill-defined borders^[43,44]. Characteristically, they demonstrate an isointense signal on T1-weighted images and an isointense to mildly hyperintense signal on T2-weighted images, with mild to moderate contrast enhancement^[43,44].

SNEC frequently exhibits aggressive invasion beyond the paranasal sinuses, involving the nasal cavity, orbits, superior/inferior orbital fissures, PPF, and optic canal^[43]. Bony erosion is also commonly observed^[43].

SINONASAL MUCOSAL MELANOMA

Sinonasal malignant melanoma (SMM) is a rare and highly metastatic tumor, accounting for approximately 1% of all malignant melanomas^[45]. Most cases originate in the nasal cavity, with the nasal septum being the most common site, followed by the lateral nasal wall. Less frequently, tumors arise in the maxillary sinus or ethmoid air cells. At the time of diagnosis, up to 40% of cases present with nodal metastases^[16,46].

The imaging characteristics of SMM often do not correlate with its biological aggressiveness, as even aggressive tumors may appear well-defined and noninvasive on scans. On CT, the appearance is typically nonspecific, as bony destruction is a common finding in many malignant tumors^[16]. On MRI, SMM usually appears hyperintense on T1-weighted and hypointense on T2-weighted images, reflecting hemorrhage and the paramagnetic effects of metal ions bound to melanin [Figure 27]^[3,47]. However, intermediate signal intensity is also frequently observed across MRI sequences. In addition, SMM has the potential for perineural spread, which may be associated with a prolonged latency period^[16,46].

SINONASAL LYMPHOMA

The head and neck region is the second most common site of extranodal lymphoma after the gastrointestinal tract. Fewer than 10% of head and neck lymphomas occur in the sinonasal cavity^[48]. Nearly all sinonasal tract lymphomas are non-Hodgkin lymphomas^[17] and can be further divided into B cell, T cell/natural killer (NK) cell, or T cell/NK precursor cell subtypes^[48]. These tumors typically appear as bulky soft-tissue masses in the maxillary sinuses or nasal cavity, often associated with necrosis and invasion of adjacent soft tissues and bony structures^[16,48].

In Western populations, Epstein-Barr virus (EBV)-negative diffuse large B cell lymphoma is the more common subtype of sinonasal lymphoma^[16,48]. In contrast, EBV-positive T/NK-cell lymphomas are more frequently observed in East Asian and South American populations^[48]. On CT imaging, sinonasal lymphomas usually appear as nonspecific, bulky, ill-defined soft-tissue masses with associated bony destruction and extension into surrounding soft tissues^[16]. On MRI, these tumors often demonstrate heterogeneous intermediate signal intensity on T1- and T2-weighted images, with moderate enhancement and restricted diffusion [Figure 28]^[16,48].

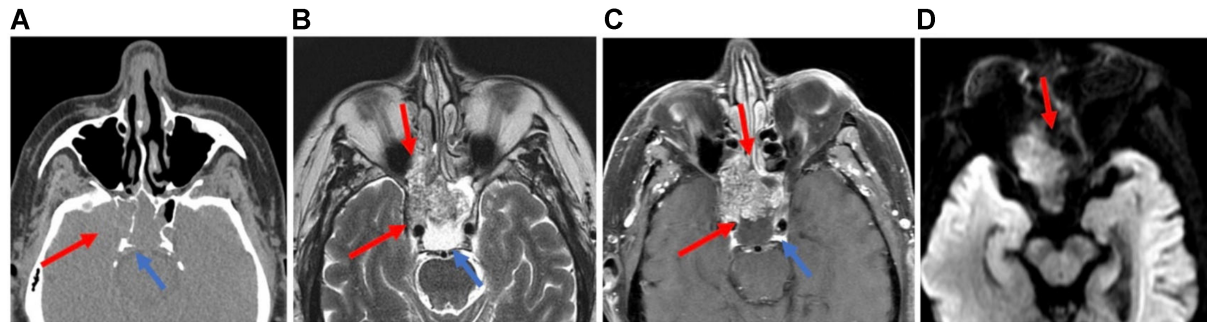


Figure 26. SMARCI-deficient sinonasal carcinoma: Axial CT (A) and Axial MRI (B-D: T2, post-contrast T1, DWI) images show an aggressive mass in the right sphenoid sinus with heterogeneous T2 intensity, restricted diffusion, and heterogeneous enhancement. The tumor destroys the sinus wall and the bony covering of the right internal carotid artery, directly invading the right cavernous sinus (red arrows). A T2-hyperintense, non-enhancing trapped secretion causes dehiscence of the sphenoid clivus along the posterior sinus wall (blue arrows). CT: Computed tomography; MRI: magnetic resonance imaging; DWI: diffusion-weighted imaging.

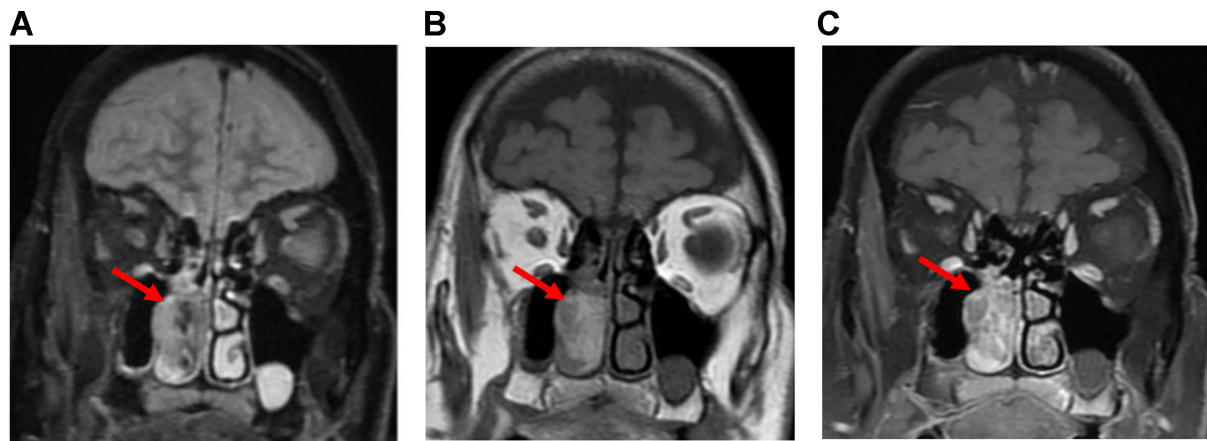


Figure 27. Sinonasal melanoma. Coronal T2 (A), precontrast T1 (B), and post-contrast T1 (C) images showing an ill-defined, T1-hyperintense, enhancing mass expanding the right nasal cavity (arrows).

Systemic staging and surveillance utilizing FDG PET/CT and DOTATATE PET/CT

MRI is preferred over CT for initial staging of sinonasal malignancies, primarily due to its superior anatomic resolution and ability to evaluate the skull base foramina. The entire neck, from the skull base through the thoracic inlet, should be included to assess for lymph node metastases. In patients with risk factors for extensive metastatic disease - such as multistation nodal involvement, lower cervical LAD, or high-grade tumor histology - FDG PET should be considered to evaluate for distant metastases. FDG PET is also highly sensitive for detecting metastatic LAD within the head and neck. Its use is particularly valuable in patients where definitive pre-treatment identification of metastatic adenopathy is critical, such as those for whom a bilateral neck dissection might be avoided or those planned for definitive radiotherapy alone. In patients with proven recurrence, FDG PET can complement or even replace conventional MRI-based anatomic imaging^[49].

Currently, no formal recommendations exist for post-treatment imaging in patients with isolated local disease, where clinical follow-up remains the primary method for detecting recurrence. However, in patients with locoregionally advanced disease, both MRI and FDG PET should be performed 3-6 months after treatment to establish a new baseline and assess treatment response. While anatomic imaging may be

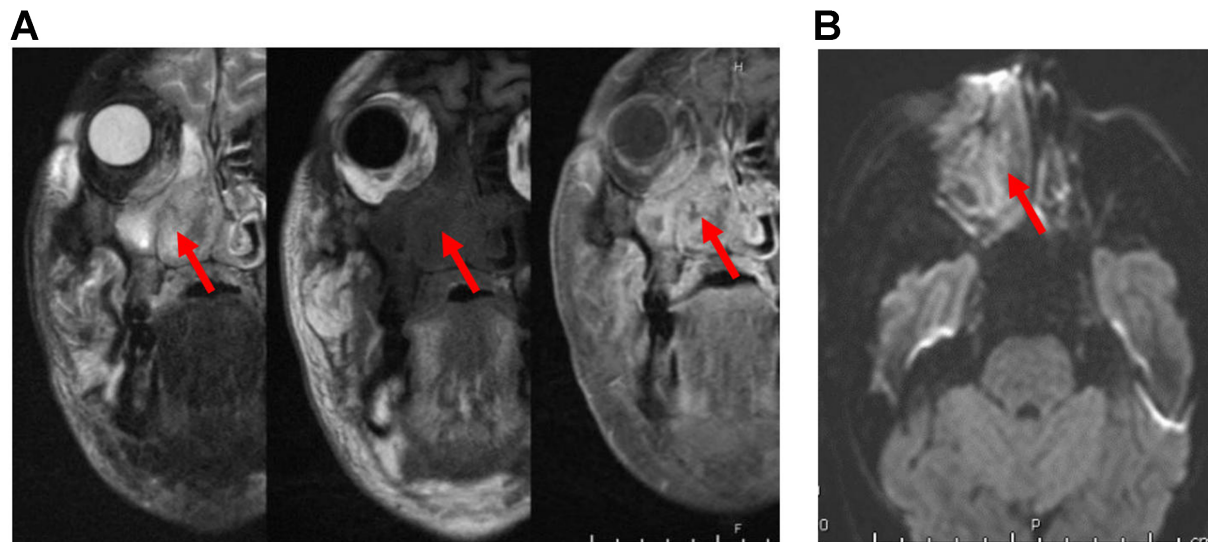


Figure 28. Sinonasal lymphoma. (A) Coronal MRI images (from left to right: T2, precontrast T1, and post-contrast T1) show an ill-defined, trans-spatial lesion with intermediate T1/T2 signal intensity and heterogeneous enhancement. The lesion extends along the nasal cavity, maxillary sinus wall, maxillary alveolus, and hard palate, with invasion of the adjacent medial right orbit and extensive stranding of the facial soft tissues (arrows); (B) Axial DWI images demonstrate a hyperintense signal (arrow), confirmed to represent restricted diffusion on the corresponding ADC maps (not shown). MRI: Magnetic resonance imaging; DWI: diffusion-weighted imaging; ADC: apparent diffusion coefficient.

obtained earlier in cases of suspected incomplete response, FDG PET should not be performed before three months because post-treatment inflammation may result in false positives^[49]. Furthermore, evidence suggests that sinonasal malignancies require an even longer interval - up to six months - for a reliable FDG PET baseline, as these tumors demonstrate a more prolonged inflammatory response than other head and neck cancers^[50].

Beyond six months, there is no consensus on surveillance imaging for asymptomatic patients. A study by Ho *et al.* found no clear survival benefit at three years for head and neck cancer patients undergoing FDG PET surveillance at 12 and 24 months post-treatment^[51]. However, these studies have not stratified outcomes by specific head and neck subsites (e.g., sinonasal) or histologies, and it is reasonable to suspect that the unique characteristics of sinonasal cancers may justify routine imaging follow-up. For example, sinonasal endoscopy has limited sensitivity for detecting recurrences - only 25% according to Khalili *et al.* - partly due to technical challenges from post-treatment changes, deep submucosal recurrences, and distal sites of relapse^[52]. Consequently, significant heterogeneity exists among clinicians and institutions regarding surveillance strategies beyond six months. When surveillance imaging is performed, MRI is typically the modality of choice, given its superior soft tissue contrast for the sinonasal cavity and skull base foramina^[52]. FDG PET serves as a useful adjunct when MRI findings are equivocal around the skull base, and it demonstrates greater sensitivity than US, CT, or MRI for detecting residual/recurrent disease outside this region [Figure 29]^[53]. At the primary site, however, FDG PET is limited by a high false-positive rate, with specificity reported as only 40% compared to 78%-85% for head and neck cancers overall^[50,54,55].

Recurrence of sinonasal malignancies typically occurs between 17-29 months after treatment, with most cases arising within five years^[50,56,57]. Certain histologies - including poorly differentiated carcinoma, melanoma, chondrosarcoma, and AdCC^[58,59] - may recur even later, supporting the need for prolonged, histology-specific surveillance strategies^[60].

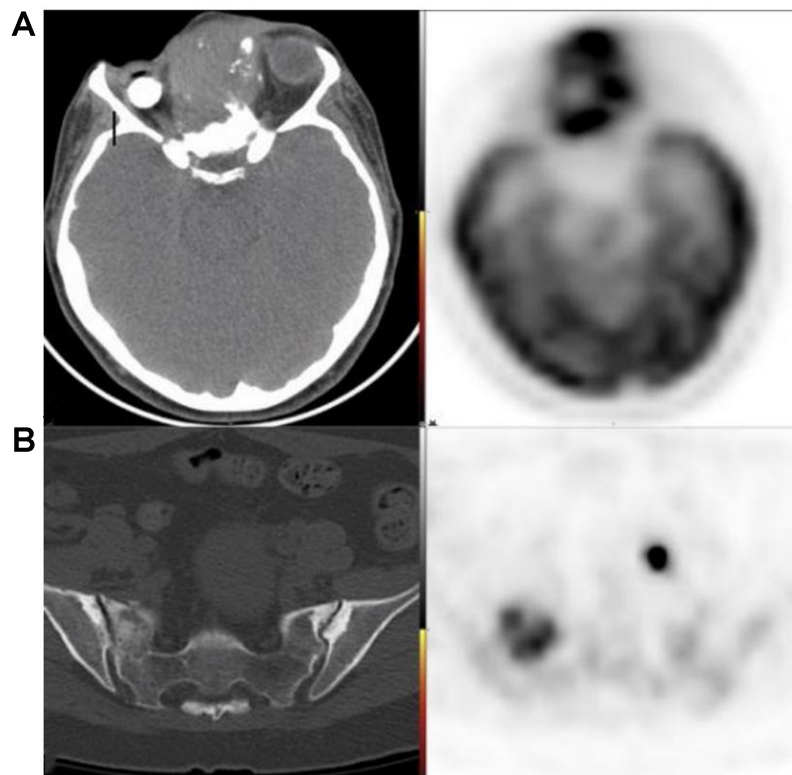


Figure 29. 49-year-old female with recurrent AdCC of the ethmoid air cells. (A) FDG PET/CT demonstrating an infiltrative, trans-spatial mass centered in the ethmoid air cells with marked FDG uptake, compatible with local recurrence; (B) FDG PET/CT in the same patient revealing distant osseous metastasis in a sclerotic right sacral ala lesion. AdCC: Adenoid cystic carcinoma; CT: computed tomography.

Neuroendocrine tumors and ENBs are uniquely avid on somatostatin receptor-based molecular imaging. Earlier neuroendocrine imaging methods, such as Ind111-octreotide planar and SPECT/CT, were limited by poor resolution and suboptimal sensitivity and specificity. The introduction of Ga68/Cu64-DOTATATE PET has significantly improved diagnostic accuracy and anatomic localization for these tumors^[61]. DOTATATE PET can therefore be considered an adjunct modality for staging and surveillance in these histologies. Although current guidelines do not include DOTATE PET for sinonasal neuroendocrine tumors - likely due to their rarity and the lack of large-scale validation studies - emerging evidence highlights specific scenarios where it is particularly useful. These include identifying primary sites of disease elsewhere in the body (e.g., gastroenteropancreatic neuroendocrine tumors with sinonasal metastasis), detecting metastatic disease not seen on CT/MRI, and evaluating situations where FDG PET is limited^[62,63]. Such scenarios include characterizing intracranial disease (where physiologic brain FDG uptake obscures lesions), distinguishing inflammatory or post-treatment changes from recurrence (both FDG-avid), and evaluating neuroendocrine neoplasms with little or no baseline FDG uptake [Figure 30].

In summary, FDG PET/CT remains the preferred modality for detecting distant metastases in epithelial tumors (e.g., SCC, adenocarcinoma) due to its sensitivity to hypermetabolic activity, whereas DOTATATE PET/CT is more suitable for neuroendocrine tumors (e.g., ENB) given its high affinity for somatostatin receptors.

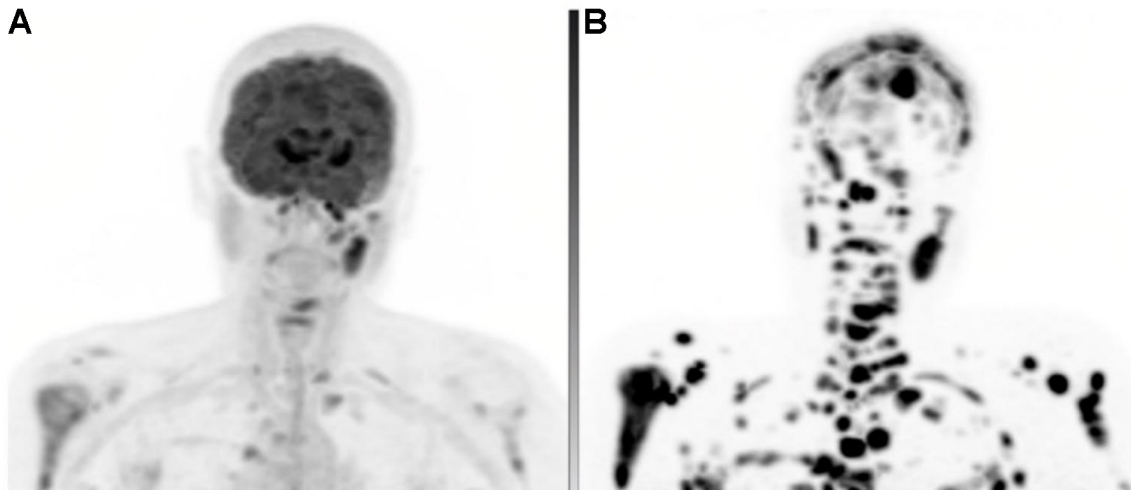


Figure 30. 56-year-old female with metastatic ENB. (A) FDG PET MIP demonstrating multiple metastatic lymph nodes and osseous lesions; (B) DOTATATE PET MIP obtained 1 month later revealing a much greater extent of metastatic disease, including numerous osseous and intracranial sites not appreciated on FDG PET. The underlying CT appearances were grossly similar, excluding the possibility that these differences were due to disease progression. ENB: Esthesioneuroblastoma; MIP: maximum intensity projection; CT: computed tomography.

CONCLUSION

The imaging features of sinonasal malignancies, combined with the use of advanced staging protocols, represent a significant step toward improving diagnostic accuracy and treatment planning. The development of advanced imaging techniques, such as FDG PET/CT and DOTATATE PET/CT, heralds a new era of enhanced diagnostic precision and a more detailed understanding of tumor behavior. Nevertheless, the rarity and heterogeneity of these tumors continue to pose challenges. These imaging modalities hold great potential for precise tumor mapping, tissue characterization, evaluation of treatment response, and monitoring for recurrence. Together with histopathological analysis and clinical assessment, they offer the prospect of a more comprehensive understanding of sinonasal malignancies and the development of more effective treatment strategies.

DECLARATIONS

Authors' contributions

Introduction, conclusion, Section "Overview of Sinonasal Tract Tumors"; initial submission: Singh V
 Section "Systemic Staging and Surveillance Utilizing FDG PET/CT and DOTATATE PET/CT": Khalaf A
 Section "Overview of Sinonasal Tract Tumors": Nguyen GK
 Section "Key Anatomy of the Skull Base and Sinuses": Fagan R
 Review of the manuscript with edits regarding surgical considerations: Su SY
 Review of the overall manuscript with edits: Learned K
 Section "CT and MR Approach to Sinonasal Tumors; revisions after submission": Hsieh KJ

Availability of data and materials

Not applicable.

Financial support and sponsorship

None.

Conflicts of interest

All authors declared that there are no conflicts of interest.

Ethical approval and consent to participate

Not applicable.

Consent for publication

Not applicable.

Copyright

© The Author(s) 2025.

REFERENCES

1. Banuchi V, Mallen J, Kraus D. Cancers of the nose, sinus, and skull base. *Surg Oncol Clin N Am.* 2015;24:563-77. DOI PubMed
2. Loevner LA, Sonners AI. Imaging of neoplasms of the paranasal sinuses. *Magn Reson Imaging Clin N Am.* 2002;10:467-93. DOI PubMed
3. Daniels DL, Mafee MF, Smith MM, et al. The frontal sinus drainage pathway and related structures. *Am J Neuroradiol.* 2003;24:1618-27. PubMed PMC
4. Laine FJ, Smoker WR. The ostiomeatal unit and endoscopic surgery: anatomy, variations, and imaging findings in inflammatory diseases. *Am J Roentgenol.* 1992;159:849-57. DOI PubMed
5. Landsberg R, Friedman M. A computer-assisted anatomical study of the nasofrontal region. *Laryngoscope.* 2001;111:2125-30. DOI PubMed
6. DeMonte F, Ginsberg LE, Clayman GL. Primary malignant tumors of the sphenoidal sinus. *Neurosurgery.* 2000;46:1084-91; discussion 1091. DOI PubMed
7. Netter FH. Netter atlas of human anatomy: classic regional approach. 8th edition. Elsevier. 2022. Available from: https://books.google.com/books?id=-ydgEAAAQBAJ&printsec=frontcover&hl=zh-CN&source=gbs_ge_summary_r&cad=0#v=onepage&q&f=false. [Last accessed on 25 Aug 2025].
8. Harnsberger HR, Osborn AG, MacDonald A, et al. Diagnostic and surgical imaging anatomy: brain, head & neck, spine. *Am J Neuroradiol.* 2007;28:795-6. PMC
9. Famuyide A, Juliano A, Moonis G. MRI of Sinonasal Malignancies. *Top Magn Reson Imaging.* 2021;30:139-49. DOI PubMed
10. Loevner LA, Sonners AI. Imaging of neoplasms of the paranasal sinuses. *Neuroimaging Clin N Am.* 2004;14:625-46. DOI PubMed
11. Madani G, Beale TJ, Lund VJ. Imaging of sinonasal tumors. *Semin Ultrasound CT MR.* 2009;30:25-38. DOI PubMed
12. Madani G, Beale TJ. Differential diagnosis in sinonasal disease. *Semin Ultrasound CT MR.* 2009;30:39-45. DOI PubMed
13. Eggesbø HB. Imaging of sinonasal tumours. *Cancer Imaging.* 2012;12:136-52. DOI PubMed PMC
14. Eisen MD, Yousem DM, Montone KT, et al. Use of preoperative MR to predict dural, perineural, and venous sinus invasion of skull base tumors. *Am J Neuroradiol.* 1996;17:1937-45. PubMed PMC
15. McIntyre JB, Perez C, Penta M, Tong L, Truelsen J, Batra PS. Patterns of dural involvement in sinonasal tumors: prospective correlation of magnetic resonance imaging and histopathologic findings. *Int Forum Allergy Rhinol.* 2012;2:336-41. DOI PubMed
16. Maroldi R, Lombardi D, Farina D, Nicolai P, Moraschi I, Pianta L. Malignant neoplasms. In: Maroldi R, Nicolai P, editors. Imaging in treatment planning for sinonasal diseases. New York, Springer-Verlag; 2005. pp. 159-220. DOI
17. Maroldi R, Farina D, Battaglia G, Maculotti P, Nicolai P, Chiesa A. MR of malignant nasosinusal neoplasms. Frequently asked questions. *Eur J Radiol.* 1997;24:181-90. DOI PubMed
18. Eisen MD, Yousem DM, Loevner LA, Thaler ER, Bilker WB, Goldberg AN. Preoperative imaging to predict orbital invasion by tumor. *Head Neck.* 2000;22:456-62. DOI PubMed
19. Agarwal M, Policeni B. Sinonasal Neoplasms. *Semin Roentgenol.* 2019;54:244-57. DOI PubMed
20. Kuan EC, Wang EW, Adappa ND, et al. International Consensus Statement on Allergy and Rhinology: sinonasal tumors. *Int Forum Allergy Rhinol.* 2024;14:149-608. DOI PubMed
21. Hawley KA, Ahmed M, Sindwani R. CT findings of sinonasal respiratory epithelial adenomatoid hamartoma: a closer look at the olfactory clefts. *Am J Neuroradiol.* 2013;34:1086-90. DOI PubMed PMC
22. Tong KN, Serra RM, Shih RY, Foss RD. Seromucinous hamartoma of the nasal cavity. *Head Neck Pathol.* 2019;13:239-42. DOI PubMed PMC
23. Chawla A, Shenoy J, Chokkappan K, Chung R. Imaging features of sinonasal inverted papilloma: a pictorial review. *Curr Probl Diagn Radiol.* 2016;45:347-53. DOI PubMed
24. Jeon TY, Kim HJ, Chung SK, et al. Sinonasal inverted papilloma: value of convoluted cerebriform pattern on MR imaging. *Am J Neuroradiol.* 2008;29:1556-60. DOI PubMed PMC
25. Agarwal A, Bhatt AA, Bathla G, et al. Update from the 5th Edition of the WHO Classification of Nasal, Paranasal, and Skull Base

- Tumors: imaging overview with histopathologic and genetic correlation. *Am J Neuroradiol.* 2023;44:1116-25. DOI PubMed PMC
26. Mishra S, Praveena NM, Panigrahi RG, Gupta YM. Imaging in the diagnosis of juvenile nasopharyngeal angiofibroma. *J Clin Imaging Sci.* 2013;3:1. DOI PubMed PMC
 27. Valkadinov I, Conev N, Dzhenkov D, Donev I. Rare case of ameloblastoma with pulmonary metastases. *Intractable Rare Dis Res.* 2017;6:211-4. DOI PubMed PMC
 28. Thawani R, Kim MS, Arastu A, et al. The contemporary management of cancers of the sinonasal tract in adults. *CA Cancer J Clin.* 2023;73:72-112. DOI PubMed PMC
 29. Hermans R, De Vuysere S, Marchal G. Squamous cell carcinoma of the sinonasal cavities. *Semin Ultrasound CT MR.* 1999;20:150-61. DOI PubMed
 30. Homma A, Hayashi R, Matsuura K, et al. Lymph node metastasis in t4 maxillary sinus squamous cell carcinoma: incidence and treatment outcome. *Ann Surg Oncol.* 2014;21:1706-10. DOI PubMed
 31. Dean KE, Shatzkes D, Phillips CD. Imaging review of new and emerging sinonasal tumors and tumor-like entities from the Fourth Edition of the World Health Organization Classification of Head and Neck Tumors. *AJNR Am J Neuroradiol.* 2019;40:584-90. DOI PubMed PMC
 32. Leivo I. Sinonasal adenocarcinoma: update on classification, immunophenotype and molecular features. *Head Neck Pathol.* 2016;10:68-74. DOI PubMed PMC
 33. Abouhanine O, Merzem A, Ndayishimiye V, et al. Sinonasal chondrosarcoma, an unusual location. *Eur J Case Rep Intern Med.* 2020;7:001933. DOI PubMed PMC
 34. Dublin AB, Bobinski M. Imaging characteristics of olfactory neuroblastoma (esthesioneuroblastoma). *J Neurol Surg B Skull Base.* 2016;77:1-5. DOI PubMed PMC
 35. Schuster JJ, Phillips CD, Levine PA. MR of esthesioneuroblastoma (olfactory neuroblastoma) and appearance after craniofacial resection. *Am J Neuroradiol.* 1994;15:1169-77. PubMed PMC
 36. Som PM, Lidov M, Brandwein M, Catalano P, Biller HF. Sinonasal esthesioneuroblastoma with intracranial extension: marginal tumor cysts as a diagnostic MR finding. *Am J Neuroradiol.* 1994;15:1259-62. PubMed PMC
 37. Navas-Campo R, Moreno Caballero L, Gasos Lafuente A, Tobajas Morlana P, Séez Valero E, Gimeno Peribáñez MJ. Olfactory neuroblastoma. Everything the radiologist should know. *Rev Argent Radiol.* 2020;84:17-29. Available from: https://www.rardigital.org.ar/_files/ugd/b2c01b_e67b8ca53e7942f0aa6cdb4888d6c2af.pdf. [Last accessed on 25 Aug 2025]
 38. Morita A, Ebersold MJ, Olsen KD, Foote RL, Lewis JE, Quast LM. Esthesioneuroblastoma: prognosis and management. *Neurosurgery.* 1993;32:706-14; discussion 714. DOI PubMed
 39. Xu CC, Dziegielewski PT, McGaw WT, Seikaly H. Sinonasal undifferentiated carcinoma (SNUC): the Alberta experience and literature review. *J Otolaryngol Head Neck Surg.* 2013;42:2. DOI PubMed PMC
 40. Phillips CD, Futterer SF, Lipper MH, Levine PA. Sinonasal undifferentiated carcinoma: CT and MR imaging of an uncommon neoplasm of the nasal cavity. *Radiology.* 1997;202:477-80. DOI PubMed
 41. Virarkar M, Saleh M, Ramani NS, Morani AC, Bhosale P. Imaging spectrum of NUT carcinomas. *Clin Imaging.* 2020;67:198-206. DOI PubMed
 42. Shatzkes DR, Ginsberg LE, Wong M, et al. Imaging appearance of *SMARCB1* (INI1)-deficient sinonasal carcinoma: a newly described sinonasal malignancy. *Am J Neuroradiol.* 2016;37:1925-9. DOI PubMed PMC
 43. Lin N, Qi M, Wang Z, et al. Small cell neuroendocrine carcinoma of paranasal sinuses: radiologic features in 14 cases. *J Comput Assist Tomogr.* 2021;45:135-41. DOI PubMed PMC
 44. Zhu Q, Zhu W, Wu J, Zhang H. The CT and MRI observations of small cell neuroendocrine carcinoma in paranasal sinuses. *World J Surg Oncol.* 2015;13:54. DOI PubMed PMC
 45. Andrianakis A, Kiss P, Pomberger M, Wolf A, Thurnher D, Tomazic PV. Sinonasal mucosal melanoma: treatment strategies and survival rates for a rare disease entity: a single center experience and review of literature. *Wien Klin Wochenschr.* 2021;133:1137-47. DOI PubMed PMC
 46. Amit M, Na'ara S, Hanna EY. Contemporary treatment approaches to sinonasal mucosal melanoma. *Curr Oncol Rep* 2018;20:10. DOI PubMed
 47. Kim YK, Choi JW, Kim HJ, et al. Melanoma of the sinonasal tract: value of a septate pattern on precontrast T1-weighted MR imaging. *Am J Neuroradiol.* 2018;39:762-67. DOI PubMed PMC
 48. Famuyide A, Juliano A, Moonis G. MRI of sinonasal malignancies. *Top Magn Reson Imaging.* 2021;30:139-49. DOI PubMed
 49. Pfister DG, Spencer S, Adkins D, et al. NCCN Clinical Practice Guidelines in Oncology (NCCN Guidelines®). Head and neck cancers. 2023. Available from: <https://nio.gov.pl/wp-content/uploads/2024/01/Wytyczne-postepowania-diagnostyczno-terapeutycznego-u-chorych-na-nowotwory-glowy-i-szyi-adaptacja-NCCN.pdf>. [Last accessed on 25 Aug 2025].
 50. Schwartz JS, Brooks SG, Stubbs V, et al. Temporal patterns of ¹⁸F-fluorodeoxyglucose positron emission tomography/computed tomography sinonasal uptake after treatment of sinonasal malignancy. *Int Forum Allergy Rhinol.* 2016;6:1301-7. DOI PubMed
 51. Ho AS, Tsao GJ, Chen FW, et al. Impact of positron emission tomography/computed tomography surveillance at 12 and 24 months for detecting head and neck cancer recurrence. *Cancer.* 2013;119:1349-56. DOI PubMed
 52. Khalili S, Worrall DM, Brooks S, et al. Endoscopy versus imaging: analysis of surveillance methods in sinonasal malignancy. *Head Neck.* 2016;38:1229-33. DOI PubMed
 53. Dunskey KA, Wehrmann DJ, Osman MM, Thornberry BM, Varvares MA. PET-CT and the detection of the asymptomatic recurrence

- or second primary lesions in the treated head and neck cancer patient. *Laryngoscope*. 2013;123:2161-4. DOI PubMed
54. Chao SS, Loh KS, Tan LK. Modalities of surveillance in treated nasopharyngeal cancer. *Otolaryngol Head Neck Surg*. 2003;129:61-4. DOI PubMed
55. Harvey RJ, Pitzer G, Nissman DB, et al. PET/CT in the assessment of previously treated skull base malignancies. *Head Neck*. 2010;32:76-84. DOI PubMed
56. Kaplan DJ, Kim JH, Wang E, Snyderman C. Prognostic indicators for salvage surgery of recurrent sinonasal malignancy. *Otolaryngol Head Neck Surg*. 2016;154:104-12. DOI PubMed
57. Tzelnick S, Levin EG, Yacobi D, Mizrachi A, Popovtzer A, Soudry E. Recurrence patterns and efficacy of surveillance modalities for sinonasal malignancies. *Am J Rhinol Allergy*. 2022;36:473-9. DOI PubMed
58. Giuffrida AY, Burgueno JE, Koniaris LG, Gutierrez JC, Duncan R, Scully SP. Chondrosarcoma in the United States (1973 to 2003): an analysis of 2890 cases from the SEER database. *J Bone Joint Surg Am*. 2009;91:1063-72. DOI PubMed
59. Kim SA, Chung YS, Lee BJ. Recurrence patterns of sinonasal cancers after a 5-year disease-free period. *Laryngoscope*. 2019;129:2451-7. DOI PubMed
60. Han AY, Nader ME, Lam K, Su SY. Current status of sinonasal cancer survivorship care. *Head Neck*. 2023;45:2458-68. DOI PubMed
61. Deppen SA, Blume J, Bobbey AJ, et al. 68Ga-DOTATATE Compared with 111In-DTPA-octreotide and conventional imaging for pulmonary and gastroenteropancreatic neuroendocrine tumors: a systematic review and meta-analysis. *J Nucl Med*. 2016;57:872-8. DOI PubMed PMC
62. Dadgar H, Norouzbeigi N, Ahmadzadehfard H, Assadi M. 68Ga-DOTATATE and 18F-FDG PET/CT for the management of esthesioneuroblastoma of the sphenoclivar region. *Clin Nucl Med*. 2020;45:e363-4. DOI PubMed
63. Liu KY, Goldrich DY, Ninan SJ, et al. The value of ⁶⁸Gallium-DOTATATE PET/CT in sinonasal neuroendocrine tumor management: a case series. *Head Neck*. 2021;43:E30-40. DOI PubMed